Marvin Glissner

Service life prediction of concrete in cold climate, benchmarking of chloride ingress simulations

Trondheim, June 2020

Nordic Master in Cold Climate Engineering

Master's thesis

NTNU

Norwegian University of Science and Technology

Faculty of Engineering

Department of Structural Engineering

Cold Climate Engineering

DTU

NTNU – Trondheim
Norwegian University of
Science and Technology

Department of Structural Engineering

Faculty of Engineering

NTNU – **Norwegian University of Science and Technology**

MASTER THESIS 2020

SUBJECT AREA:	DATE:	NO. OF PAGES:
Concrete technology	22.06.2020	69

TITLE:

Service life prediction of concrete in cold climate, benchmarking of chloride ingress simulations

BY:

Marvin Glissner

SUMMARY: Chloride ingress into concrete can lead to pitting corrosion of reinforcement steel once a critical chloride threshold is reached at the boundary of the steel surface and surrounding concrete cover. This is especially crucial in environments where a lot of chloride containing salts are present by nature or used for e.g. de-icing operations in cold climates. Reactive mass transport model that can predict ingress of such species move more and more into the focus for reliable predictions on service life of concrete structures under specific exposure conditions where chloride ingress is of major relevance. As it is of such big interest chloride ingress into concrete and cement pastes has been an area of interest for decades. The chemical aspects of chloride binding are mostly understood and commonly agreed upon by the scientific community. However, it has been shown by several authors that also physical binding on Calcium Silicate Hydrates, that form the binding part of a concrete matrix, is of big importance in considerations towards total chloride binding capacity of cementitious material. Reactive mass transport model built for concrete service life prediction do not consider this physical chloride binding at the present point. This Thesis presents two modelling methodologies that could potentially be used for consideration of physical chloride binding in a reactive mass transport model, namely by means of a modified Langmuir isotherm approach and a surface complexation approach. The possible implementation of the modified Langmuir isotherm has been tested for a reactive mass transport model. Implementation before and after a chemical solver is run, was tested in this sequenced single step model. The used model framework has been developed at the Technical University of Denmark (DTU). The results received under consideration of laboratory data obtained from published studies show that in the used model the predictions by means of a modified Langmuir isotherm would always lead to an over- or underestimation of true physical bound chlorides. Hence the modified Langmuir isotherm approach could only be used to hint a direction but needs careful interpretation of results. A better solution might be the implementation of a surface complexation term. No implementation by means of a surface complexation approach was included or compared to results within this work as this was not the primary focus. Surface complexation modelling remains interesting and promising based on the theoretical background and methodology presented in this Thesis.

RESPONSIBLE TEACHER: Prof. Dr. Mette Rica Geiker (NTNU)

SUPERVISOR(S): Prof. Dr. Mette Rica Geiker (NTNU), Prof. Dr. Alexander Michel (DTU), Dr. Victor Marcos Meson(DTU)

CARRIED OUT AT: department of structural engineering of the Norwegian University of Science and Technology (NTNU)

Preface

The work presented here is a part of the joint MSc degree in Cold Climate Engineering, carried out at the department of structural engineering of the Norwegian University of Science and Technology (NTNU) in the spring semester of 2020. The thesis has been conducted in collaboration with the department of civil engineering of the Techcnical University of Denmark (DTU). The main supervisor at NTNU was Prof. Dr. Mette Rica Geiker. DTU supervisor was Prof. Dr. Alexander Michel, with co-supervision of postdoc Dr. Victor Marcos Meson. The time frame of this work was 20 weeks as stated in the thesis regulations of the Norwegian University of Science and technology. Due to cancellation of meetings after travelling abroad from Norway to Denmark, the Thesis work has been extended by three additional weeks, when a nation wide shut down was decided by the government after a global virus outbreak. The idea to work on this topic arose during brainstorming about potential areas of interest with Dr. Mette Geiker after first arrival in Norway in August 2019.

Acknowledgment

Abstract

Chloride ingress into concrete can lead to pitting corrosion of reinforcement steel once a critical chloride threshold is reached at the boundary of the steel surface and surrounding concrete cover. This is especially crucial in environments where a lot of chloride containing salts are present by nature or used for e.g. de-icing operations in cold climates. Reactive mass transport model that can predict ingress of such species move more and more into the focus for reliable predictions on service life of concrete structures under specific exposure conditions where chloride ingress is of major relevance. As it is of such big interest chloride ingress into concrete and cement pastes has been an area of interest for decades. The chemical aspects of chloride binding are mostly understood and commonly agreed upon by the scientific community. However, it has been shown by several authors that also physical binding on Calcium Silicate Hydrates, that form the binding part of a concrete matrix, is of big importance in considerations towards total chloride binding capacity of cementitious material. Reactive mass transport model built for concrete service life prediction do not consider this physical chloride binding at the present point. This Thesis presents two modelling methodologies that could potentially be used for consideration of physical chloride binding in a reactive mass transport model, namely by means of a modified Langmuir isotherm approach and a surface complexation approach. The possible implementation of the modified Langmuir isotherm has been tested for a reactive mass transport model. Implementation before and after a chemical solver is run, was tested in this sequenced single step model. The used model framework has been developed at the Technical University of Denmark (DTU). The results received under consideration of laboratory data obtained from published studies show that in the used model the predictions by means of a modified Langmuir isotherm would always lead to an over- or underestimation of true physical bound chlorides. Hence the modified Langmuir isotherm approach could only be used to hint a direction but needs careful interpretation of results. A better solution might be the implementation of a surface complexation term. No implementation by means of a surface complexation approach was included or compared to results within this work as this was not the primary focus. Surface complexation modelling remains interesting and promising based on the theoretical background and methodology presented in this Thesis.

Contents

Abbreviations and list of symbols

Cement paste	Cement + water
Binder	Cement + cement substitute
C-S-H	Calcium Silicate Hydrate
XRD	X-ray diffraction
TGA	Thermogravimetric analysis
Si MAS NMR	Silicon Magic Angle Spinning Nuclear Magnetic Resonance
wt.%	Weight percentage
C_3S	Alite
C_2S	Belite
C_3A	Tricalciumaluminate
C_4AF	Tetracalciumaluminateferrit
Ca/Si	Ratio of calcium to silicon [-]
w/c	Ratio of water to cement [-]
w/b	Ratio of water to binder [-]
ζ_d	relative dielectricity coefficient [-]
ζ_0	dielectricity coefficient in vacuum [-]
P_c	capillary pressure [Pa]
P_v	vapour pressure [Pa]
C	moisture capacity [g/g]
R	universal gas constant [-]
Θ	relative moisture content [g/m^3]
φ	relative humidity [%]
ρ	Density [g/cm^3]
f	scaling factor [-]
T	Temperature in kelvin [k]
μ_{dry}	dry-cup vapour diffusion resistance factor [-]
S_l	degree of saturation [%]
C_{Cl}	chloride concentration [mol/l]
D_{Cl}^0	ionic diffusion coefficient chloride [$\mu m^2/s$]
D	effective diffusion coefficient [$\mu m^2/s$]
A	Ionic activity [-]
Z	Valence [-]
M	Molar mass [g/mol]
V	Volume [l]
m	Mass [g]
K	equilibrium constant [-]
Ψ_o	Surface potential [V]
a	Activity of chemical species [-]
F	Faraday constant [C/mol]
N	Number of moles [mol]
α	Bindin parameter α [-]
β	Bindin parameter β [-]
σ	Chare density [C/m^2]
μ	Ionic strength [mol/l]

1. Introduction

If reinforcement steel in a reinforced concrete structure is exposed to chlorides this might induce pitting corrosion. To initiate pitting a certain amount of chlorides has to reach the steel through the concrete micro-structure. There are various sources of chlorides. Chlorides are for example present in seawater but often structures are also exposed to de-icing salts. Especially in cold regions like Norway road authorities use extensive amounts of chloride containing salts to keep the infrastructure ice free (see e.g. (Vignisdottir *et al.*, 2016)). If a corrosion process is initiated by the free chlorides in the pore solution it will alter the steel and lead to a deterioration of the structural integrity. Thus, chloride ingress into concrete structures is an important factor to determine the service lifetime of a given structure which suffers from chloride exposure. Ingress mechanisms are not trivial and are influenced by a huge variety of factors. The simplified diagram by Fidjestöl and Tuutti shows that two concrete mixes will have different chloride threshold values and consequently require a different concrete cover for the same service life (Fidjestöl and Tuutti, 1995):
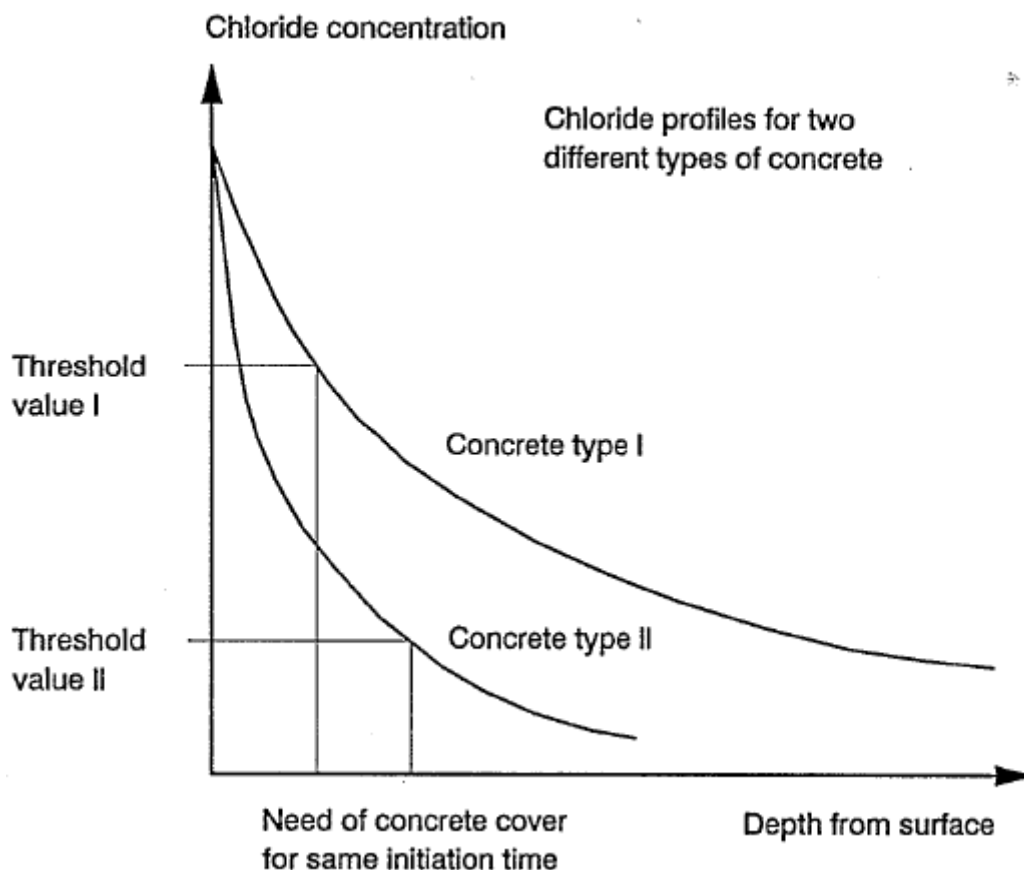

Figure 1: Schematic sketch of corrosion initiation depth for two different concretes (Fidjestöl and Tuutti, 1995)

To have a tool aiding in determination of the service lifespan different model approaches have been developed over time as for example shown in (Baroghel-bouny *et al.*, 2012). An interesting feature of Calcium Silicate Hydrates, the main product of cement hydration, is the ability to physically bind chlorides. This physical binding occurs without formation of additional chemical species and is most often not included in service life determination. In this study an existing multi-physical model framework is used to predict chloride ingress under certain conditions.

1.1. Strengths/limitations

The used model framework includes moisture as well as ionic transport and couples it with chemical reactions to resemble the material structure of the investigated mixture and gives an idea of the transport properties and ionic concentrations of different species at a given age and depth in the material. The weakness of this framework at this time is the absence of physical binding in the considerations and high dependency on correct input assumptions.

1.2. Objective

Therefore, the objective of this master thesis is to implement the physical binding phenomena into the existing model framework. This goal should be reached by:

1. Proposing a methodology for modelling of physical chloride binding based on existing literature
2. Find existing data on the topic of physical chloride binding, review it and calibrate the chosen method with the reviewed data
3. Investigating the impact of the modelling sequence in a single step sequenced model on the results

2. Theoretical background

2.1. Chloride binding capacity

The chloride binding capacity describes the ability of the cement hydration products to bind chloride ions. Chlorides can be present as free chloride in the pore solution as well as bound chlorides, either chemically or physically bound (Glasser, Marchand and Samson, 2008).

There are opposing reports on the exact importance of physical and chemical binding capacities. Binding mechanisms are e.g. dependent on the Ca/Si ratio of the C-S-H gel, the pH value of the given exposure phase and chloride concentration as mentioned in (Shi, Geiker, Lothenbach, *et al.*, 2017a). Many authors like Hirao et al. report chloride bound physical to C-S-H but do not provide a model or thorough explanation for this observation (Hirao *et al.*, 2005). Even though there has been extensive work done in the general field of chloride binding within the last decades, literature is more scarce for the physical chloride binding phenomena and comparison due to differences in many parameters such as the material, exposure conditions, handling of experiments, etc. can be troublesome.

It is commonly accepted in the research community that chemical binding can be attributed to the reaction of the C_3A and C_4AF phases and followed formation of Fe-Friedel's salt (iron containing) ,Friedel's salt ($Ca_4Al_2Cl_2(OH)_{12} \cdot 4H_2O$) and Kunzel's salt ($Ca_4Al_2Cl(SO_4)_{0.5}(OH)_{12} \cdot 6H_2O$). Where the Friedel's salt formation is of greater importance for common concrete service environments (Baroghel-bouny *et al.*, 2012).

The physical binding is mainly governed by surface complexation and electrostatic interaction on the C-S-H surface as will be discussed in Section 2.1.1. The cation, depending on the chloride salt (e.g. $Ca^+ \ Na^+ \ Li^+$), has been shown to not only have an impact on the general binding but also on the physical binding capacity (Hencoq, 2006). Tang and Nilsson showed that the chloride binding capacity is dependent on content of C-S-H gel in concrete (Tang and Nilsson, 1993). According to their report the chloride binding capacity can be described by a Freundlich equation for exposure concentrations higher than 0.01 mol/l of chlorides. For concentrations smaller than 0.05 mol/l an isotherm following the Langmuir type has been proposed. Assuming the binding capacity can be described by a Langmuir isotherm it can be written as shown in Eq.1 (Michel, 2012):

$$D_{Cl,bind}(S_l) = D_{Cl}^0(S_l)\frac{1}{1 + \alpha_{binder}/(\theta_l(1 + \beta_{binder}C_{Cl})^2)} \qquad \text{Eq.1}$$

According to (Glass and Buenfeld, 2000) the α and β value are binding constants and dependent on the chloride concentration C_{Cl} and exposed material. It should be stated that the early approach given by Tang and Nilsson does not distinguish between physical and chemically bound chlorides (Tang and Nilsson, 1993).

2.1.1. Physical chloride binding

In this thesis report as stated in the objectives (Section 1.2) the focus is given on physical chloride binding. Therefore, a more in-depth explanation of physical chloride binding is required.

According to Plassard et al. adsorption of chlorides can be explained by Van-der-Waals forces and electrostatic interactions between chlorides and the surface of C-S-H phases, surface charge plays thereby an important role and is created by dissociation of silanol $SiOH$ surface groups which can vary in their dissociation degree from ten to ninety percent (Plassard *et al.*, 2005). The work of Plassard et al. forms the basis for more sophisticated efforts towards physical binding with a series of papers from Elakneswaran et al. (Elakneswaran, Nawa and Kurumisawa, 2009)(yoga *et al.*, 2010) (Yogarajah, Nawa and Kurumisawa, 2018).

The main mechanism that is considered here to cause surface charge on the C-S-H surface is the deprotonation as shown in following chemical reaction (Helene Viallis-Terrisse, Andre Nonat, 2001; Elakneswaran, Nawa and Kurumisawa, 2009):

$$\equiv SiOH + OH^- \Longleftrightarrow \equiv SiO^- + H_2O$$

Eq.2
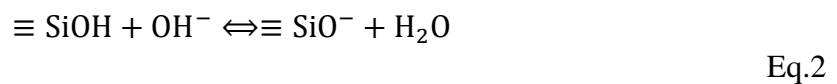
The authors calculate the deprotonation constant by:

$$K_{OH} = \frac{a_{SiO^-}}{a_{SiOH} \cdot a_{OH^-}} \exp\left(-\frac{F\Psi_o}{RT}\right)$$

Eq.3

Where K_{OH} is the intrinsic equilibrium constant for deprotonation, a is the activity of the species, Ψ_o is the surface potential $[V]$, R is the universal gas constant, and T is the temperature [k].

Furthermore chlorides are considered to bind (ionic) to unionized silanol groups by (Elakneswaran, Nawa and Kurumisawa, 2009):

$$\equiv SiOH + Cl^- \Leftrightarrow \equiv SiOHCl^-$$
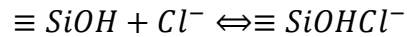
However, Plusquellect and Nonat report in their study, based on experiments with synthetic C-S-H suspension (varying Ca/Si ratios between 0.8 and 1.42), that chlorides do not **adsorb** on C-S-H particles but rather accumulate in the diffuse layer surrounding C-S-H when competing with OH^- ions in aqueous solution (Plusquellec and Nonat, 2016). Even though different approaches to explain this chloride binding, which cannot be attributed to chemical binding, exist, the general agreement that can be found between different authors is the importance of charge distribution on and around calcium silicate hydrates. Terms like "zeta potential", "surface potential" or "diffuse layer" are often used in that perspective requiring a basic explanation of those terms to clarify their meaning.

If cement particles and hydrate phases are exposed to liquid solution they are surrounded by an electrical double layer. The Stern model is a widely accepted model and can be used to help explain this electrical double layer (Stern, 1924). The Stern model combines earlier models of Helmholtz (1897) Gouy (1910) and Chapman (1913). In the model interpretation by Stern, a particle surface charged with a negative surface potential (Nernst potential) will be surrounded by a layer of adsorbed anions. This layer of anions is called the inner Helmholtz-layer. It forms due to high Van-der-Waals forces between the anions, which are bigger than the electrostatic repelling forces (Leidheiser, 1981). Following on the inner Helmholtz-layer is the outer Helmholtz-layer. This layer is formed by cations. Due to their size and the hydration hull these cations are connected to the surface by electrostatic forces. The potential which increases between the true surface and inner Helmholtz-layer therefore decreases in the outer Helmholtz layer. The inner and outer layer together are called Stern layer. Because of their bigger required volume within the layer the cations are not able to neutralize the whole negative charge created by anions. The compensation therefore happens by formation of a **diffuse ion layer** around the particle. The concentration of cations in the diffuse layer decreases exponentially with respect to the distance of the surface. On the other hand the concentration of negative charged ions increases with distance eventually the compensation of charge is reached. The point where the charge balance is reached marks the end of the diffuse layer. Stern and diffuse layer are combined in the expression **electrical double layer** (Müller, 1996). The true surface potential and the Stern potential are not directly measurable. By applying a current a part of the diffuse layer can be sheared away and this way a potential be measured. There are different ways to

shear the diffuse layer. The measured potential at the shear plane is called **zeta potential**. The zeta potential is dependent on the distance between shear plane and particle surface and with different measuring methods different values will be measured (Müller, 1996). Figure 2 illustrates the double layer model:
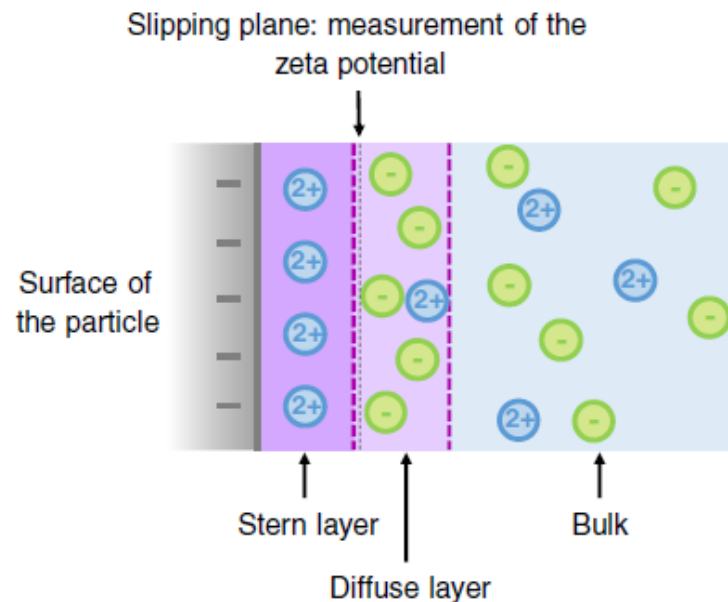
Figure 2: Electrochemical double layer model (Plusquellec and Nonat, 2016)

Other influences on the zeta potential are the ion concentration in the solution and the size of particles. Because of that and a huge variety of different measurement equipment, a quantitative comparison of studies can be quite challenging. If the ion concentration increases, the diffuse layer will be denser. If a constant shear distance is assumed, a smaller zeta potential will be measured. In high concentrations of electrolytes, charge can be neutralized in the diffuse layer which would lead to no possible measurement of the zeta potential (Alkan *et al.*, 2005). This double layer model explains why factors such as ion concentration and pH-value of solution as well as associated cation have an influence on physical binding capacities.

Tritthart reports that the physical binding of Cl^- increases with decrease of OH^- concentration. Meaning a decrease in pH leads to increased binding of chlorides. In his perception the chlorides compete with hydroxyl ions for charge compensation (Tritthart, 1989). In Tritthart's study the chlorides were introduced into the mixing water, which might cause additional impacts on samples compared to exposure of (chloride free) cured samples to a chloride containing exposure solution. The main conclusions of studies by Weerdt et al. and Shi et al. are that there is no major difference in Friedel's salt amounts, which accounts for the majority of chemical binding if different exposure solutions with same chloride content are used on well hydrated

samples. But the associated cation shows a big impact (Weerdt *et al.*, 2015)(Shi, Geiker, De Weerdt, *et al.*, 2017a). Figure 3 illustrates results from (Shi, Geiker, De Weerdt, *et al.*, 2017a), indicating that the associated cation has a huge influence on the **physical** chloride binding. The figure shows the amount of chloride adsorbed onto the C-S-H on the ordinate and the concentration of the exposure solution on the abscissa. If samples are exposed to a solution containing $CaCl_2$ the physical binding is, with increasing exposure concentration, increased compared to exposure to a $NaCl$ solution.

In the previously mentioned study, (Weerdt *et al.*, 2015) showed that a linear relationship between bound chloride and pH value can be drawn for exposure to $CaCl_2$ and $MgCl_2$ solutions but not for exposure to $NaCl$ solutions. It was predicted by thermodynamic modelling that exposure to $CaCl_2$ and $MgCl_2$ solutions leads to precipitation of the associated salts $Ca(OH)_2$ and $Mg(OH)_2$, which in return decreases pH and increases solubility of Ca as shown in Figure 4.
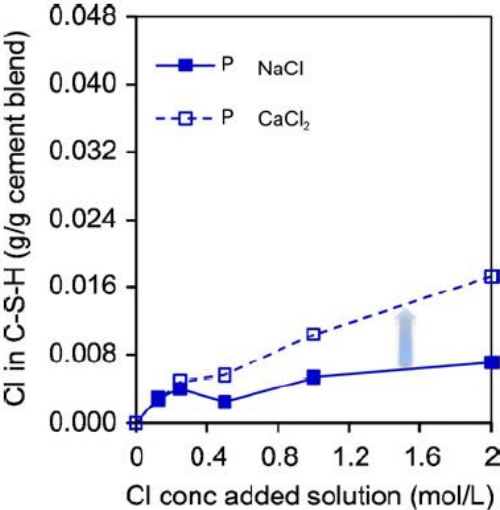
Figure 3: Physical chloride binding dependent on exposure solution (Shi, Geiker, De Weerdt, *et al.*, 2017a)
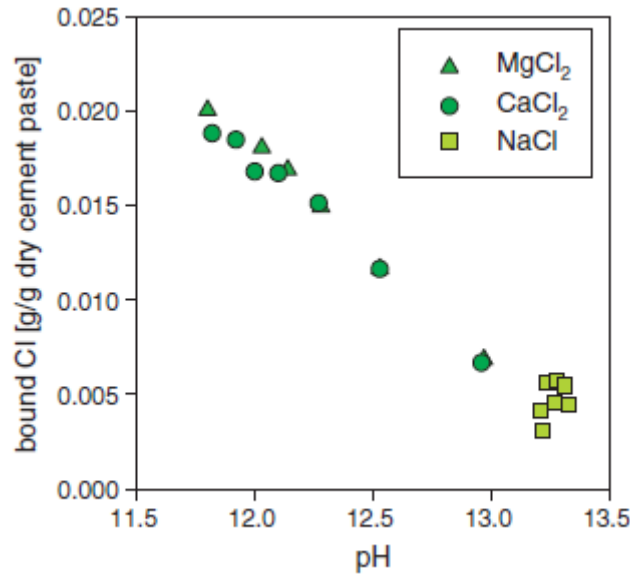
Figure 4: Bound chlorides vs pH in paste, different exposure solutions (Weerdt *et al.*, 2015)

This affects the Ca/Si ratio of the C-S-H itself. In previous studies summarized in a literature review by Nonat it has been reported that the structure of C-S-H is highly dependent on the Ca/Si ratio (Nonat, 2004) so is the silicate mean chain length. An increasing Ca/Si ratio leads to a decreased silicate chain length (Richardson, 2004). At high Ca/Si ratios however, the mean chain length does not vary much anymore (Ping Yu, R. James Kirkpatrick, Brent Poe, 1999). An explanation could be that with Ca/Si ratios above approximately 1.3 entire silicate chain segments substitute OH and create OH groups balanced by Ca rather than Si (Chen *et al.*, 2004). In De Weerdts study it is shown that more chloride can be associated with C-S-H phases containing a higher Ca/Si ratio. Exposure to $NaCl$ solution did not show altering of the C-S-H phases, these findings are backed not only by modelling but also experimental work (Weerdt *et al.*, 2015). Inversion of the surface charge (often referred to as overcharging) of C-S-H is another factor. Heath and Ilett concluded by charge modelling that the surface potential becomes positive at high Ca/Si ratios and negative at lower Ca/Si ratios. (Heath, T. G., D. J. Ilett, 1996). Labbez et al. on the other hand backed simulations with experimental work showing that in a C-S-H suspension with high Ca concentrations Ca^{2+} ions accumulate on the C-S-H surface and lead to a reversal of the surface charge (Labbez *et al.*, 2007). Their simulation data fit well without a fitting factor to experimental electrophoretic measurement data. In their simulation, they only assumed the earlier mentioned dissociation of silanol sites to determine charge.

$$\equiv SiOH + OH^- \Longleftrightarrow \equiv SiO^- + H_2O$$
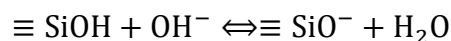
This indicates that the theory-based simulation has a sound physical basis (Labbez *et al.*, 2007). The positive charge due to overcharging might increase the ability to bind negative charged chloride ions. Good agreement between experimental zeta potential measurements focusing on degradation of hydrated cement paste and modelling of the same considering deprotonation of the mentioned silanol surface sites and a calcification reaction:

$$\equiv SiOH + Ca^{2+} \Leftrightarrow \equiv SiOCa^{2+} + H^+$$
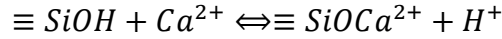
as practiced by Pointeau et al. further helps to understand charge evolution and shows applicability of theoretical approaches on the surface complexation (Pointeau *et al.*, 2006).

Deprotonation and surface complexation due to Calcium adsorption are not the only reactions that should be considered when talking about surface complexation and physical chloride binding. Also other ions such as Na^+, K^+, Cl^- and So_4^{2-} are able to bind to silanol surface sites (Hosokawa *et al.*, 2006). Following reactions can therefore be of importance in those complexation processes:

$$\equiv SiOH + Na^+ \Leftrightarrow \equiv SiONa + H^+$$

$$\equiv SiOH + K^+ \Leftrightarrow \equiv SiOK + H^+$$

$$\equiv SiOH + Ca^{2+} + Cl^- \Leftrightarrow \equiv SiOCaCl + H^+$$

$$\equiv SiOH + Ca^{2+} + SO_4^{2-} \Leftrightarrow \equiv SiOCaSO_4^- + H^+$$
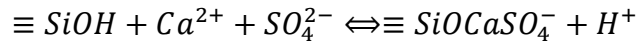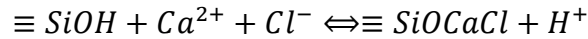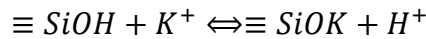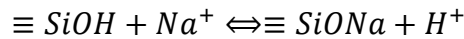
As the adsorption of cations appears on the surface sites, one important factor is the number of surface sites in the C-S-H. Terisse and Nonat estimate this number by a structural model of C-S-H (Helene Viallis-Terrisse, Andre Nonat, 2001). In the model proposed by Taylor a jennite-like structure is thought to be predominant in C-S-H with high Ca/Si ratio (Taylor, 1993). Contradicting Cong and Kirkpatrick propose a mainly tobermorite-like structure as main type of C-S-H with a Ca/Si ratio below 1.5 (Cong and Kirkpatrick, 1996). Considering the tobermorite-like structure a CaO_2 sheet is bound on each site with a silicate chain. In the chain every third tetrahedron is present as a bridging part, where the end of chains consist of the silanol site and the bridging sites of siladinol $Si(OH)_2$ (Nonat, 2004)(Pointeau *et al.*, 2006)(Richardson, 2004). The mentioned studies do not consider siladinol in surface complexation processes. With a specific surface area of 500 m^2g Viallis-Terrisse and Nonat calculated a surface site density based on the tobermorite-like structure model of 4.87 $sites/nm^2$ (Helene Viallis-Terrisse, Andre Nonat, 2001). These values are also used by other authors (Elakneswaran, Nawa and Kurumisawa, 2009)(Pointeau *et al.*, 2006).

As has been shown, physical binding is a topic based on many factors crossing borders of different research disciplines. Current theoretical assumptions lead to comparable results with experimental work. However, focus diverge in the different studies and therefore a lack of quantitative comparison exists. The main mechanisms seem to be explainable with sound physical basis but important factors such as surface site density may need further investigation.

2.2. Reactive Mass Transport model

The Reactive Mass Transport model used in this thesis report (RMT) is a multi-physical model accounting for mass transport, chemical reactions, microstructure and hydration processes. Those are the key components to be able to predict ingress of a specific chemical species. The model framework was developed on basis of the work by (Jensen, Johannesson and Geiker, 2014) and (Johannesson, 2010), to be able to simulate transport in cementitious systems. Coupling it with e.g. limiting factors for a specific ionic species at a given ingress depth and time, the prediction of the service life of a given structure becomes possible. Following schematic diagram, introduces the main components of the framework. As the schematic overview shows, the model consists of three main modules. One module for mass transport calculations, one module solving the occurring chemical reactions, and another module describing and calculating the pore structure. The mass transport properties are split in three groups: ionic transport, moisture transport, and gas transport.

The Ionic transport is determined by advection, diffusion and electro-migration. The part considering moisture transport is dependent on the degree of saturation and capillary transport mechanism as will be elaborated in section 2.2.3. The gas transport is based on diffusion. All of these transport mechanisms are connected and require an input of initial transport properties of the porous system. Ionic transport will lead to a specific ionic concentration and potential in the pore solution. Moisture transport influences the ionic transport by advection, but it will also change the moisture content and therefore the pore saturation, the capillary pressure and relative humidity are affected as they all are parameters connected to each other. The resulting pore solution and moisture content lead to an equilibrium state. In this equilibrium state a specific ionic concentration and water content are reached depended on the transport conditions.
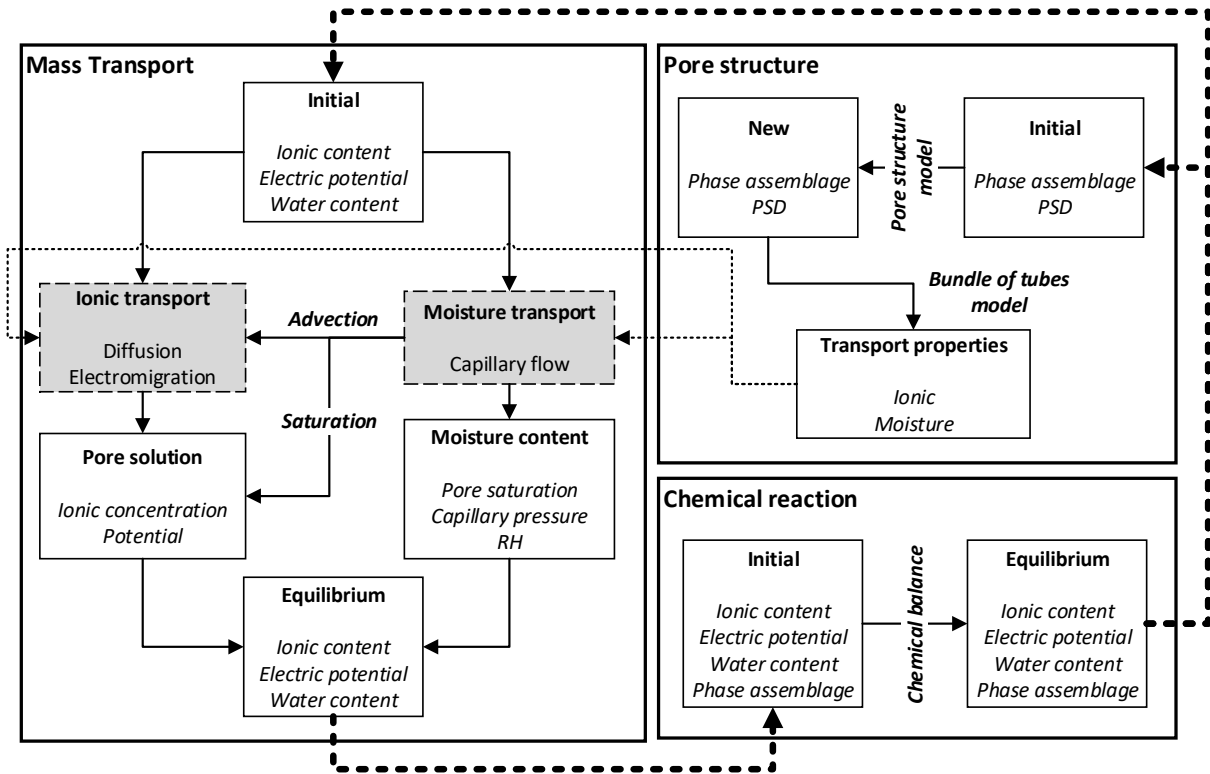
Figure 5: Schematic overview of the framework (Meson, 2019)

This equilibrium state with its parameters and an initial phase assemblage of the cementitious system is transferred to the chemical solver function. The chemical solver balances the given system in terms of chemical equilibria. The output is a new ionic concentration, water content and phase assemblage. The new information is not only fed back into the mass transport module where it changes the initial conditions but also into the pore structure module. The pore structure module requires an initial pore size distribution and phase assemblage. With the initial conditions a new pore size distribution is calculated and new transport properties for ionic and moisture transport are derived. These transport properties are fed back into the mass transport part.

2.2.1. Governing equation set describing the mass transport

The mass transport is based on the solution of a Poisson-Nernst-Planck equation system "PNP-system". In a PNP equation system the Planck-Nernst equation generally describes the diffusion of ions by using an ionic concentration- and electrical potential gradient which is coupled to the Poisson part. The latter determines the electrical potential and is based on Gauss law. Extension of the PNP system in terms of a moisture inclusion is necessary as otherwise only diffusion and migration would be considered but no advection (Michel *et al.*, 2019). The extended PNP system takes the following shape:

$$\varepsilon^l \frac{\partial c_i^l}{\partial t} + c_i^l \frac{\partial \varepsilon}{\partial t} = \nabla \left(D_i^l \varepsilon^l \nabla c_i^l + D_i^l c_i^l \nabla \varepsilon^l - A_i^l Z_i \varepsilon^l c_i^l \nabla E \right) + v^{l,s} \varepsilon^l \nabla c_i^l$$
$$+ v^{l,s} c_i^l \nabla \varepsilon^l + q_i$$

Eq.4

With: Indices being $l = liquid\ phase, s = solid\ phase, i = constituent\ i$, ε is the saturation, c the concentration, D the effective diffusion coefficient, A the ionic activity, Z is the valence of the constituent, E is the electrical potential, $v^{l,s}$ the velocity of the liquid along the solid and q_i a chemical equilibrium term (Jensen, Johannesson and Geiker, 2015).

The ionic activity A is described as

$$A_i^l = \frac{D_i^l\ F}{R\ T}$$

Eq.5

($F = Faraday\ constant\ R = as\ constant\ T = temperature\ in\ kelvin$)

the velocity as

$$v^{l,s} = -D_{\varepsilon^l} \nabla \varepsilon_i^l$$

Eq.6

and the electrical potential by:

$$\zeta_d \zeta_0 \nabla^2 E = F \sum_{i=1}^{n} c_i z_i$$

Eq.7

$\zeta_d = relative\ dielectrictiy\ coefficient, \zeta_0 = dielectricity\ coefficient\ in\ vacuum$

2.2.2. Chemical equilibrium

The term q_i for the chemical equilibrium is solved using the PHREEQC code (Parkhurst and Appelo, 2013), which allows for a wide variety of aqueous geochemical calculations. In the RMT model, equilibrium between the solid and liquid phase, vapour and liquid phase as well as in the liquid phase between the ionic species can be considered (Addassi *et al.*, 2019).

In connection with a thermodynamic database for hydrated cements and alkali activated materials, Cemdata18 (Lothenbach *et al.*, 2019), the chemical equilibrium solver is able to predict the assemblage of the different hydrate phases forming in the hydrating cement paste. All common cement hydrates can be considered, and the database is valid for temperatures in the range between 273 to 373 Kelvin. Chemical binding in the modelled system is considered in terms of formation of Friedel's salt $(Ca_4Al_2Cl_2(OH)_{12} \cdot 4H_2O)$ and Kunzel's salt $(Ca_4Al_2Cl(SO_4)_{0.5}(OH)_{12} \cdot 6H_2O)$. The following dissolution reactions are used to calculate the solubility products (Lothenbach *et al.*, 2019):

Friedel's salt:

$$Ca_4Al_2Cl_2(OH)_{12} \cdot 4H_2O \rightarrow 4Ca^{2+} + 2Al(OH)_4^- + 2CL^- + 4OH^- + 4H_2O$$

Fe-Friedel's salt:

$$Ca_4Fe_2Cl_2(OH)_{12} \cdot 4H_2O \rightarrow 4Ca^{2+} + 2Fe(OH)_4^- + 2CL^- + 4OH^- + 4H_2O$$

Kuzel's salt:

$$Ca_4Al_2Cl(SO_4)_{0.5}(OH)_{12} \cdot 6H_2O$$
$$\rightarrow 4Ca^{2+} + 2Al(OH)_4^- + Cl^- + 0.5\,SO_4^{2-} + 4OH^- + 6H_2O$$
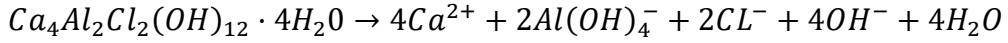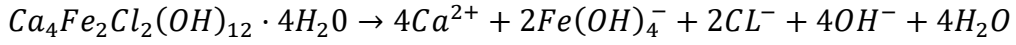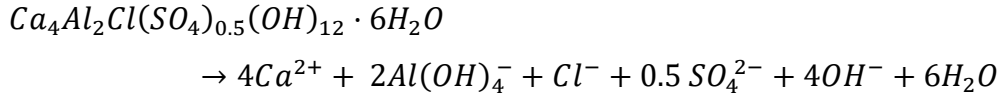
2.2.3. Moisture content and pore structure model

The porous microstructure and resulting flow properties are included based on an approach by Scheffler and Plagge (Scheffler and Plagge, 2010) that describes it as a bundle of tubes. This semi-analytical-empirical model couples a physical basis with a mechanistic description, requiring only basic material properties as input parameters.

In the mechanistic description, the model distinguishes between serial and parallel transport. As both transport coefficients for the liquid and for the vapour phase are dependent on the saturation degree, as will be seen later, a great variety of moisture contents can be pictured by this approach without loss of modelling accuracy (Scheffler and Plagge, 2010). Figure 6 illustrates the mechanistic approach. If the moisture content is low, vapour diffusion will be dominating the transport properties and the number of tubes contributing to parallel transport considered in the model will be low. This makes a lot of sense as the amount of water required to form one monolayer inside a pore of hardened cement paste is reached at around approximately 12% relative humidity (Brunauer, Emmett and Teller, 1938). On the other hand, if the moisture content is high, liquid flux will be the dominating transport mechanism. With increasing relative vapour pressure, subsequently more and more pores will fill up by capillary condensation and micropore filling (Lippens, Linsen and Boer, 1964). Liquid filled pores become connected and parallel liquid transport becomes possible in an increasing number of pores. Contribution of serial and parallel transport in the different transport coefficients varies.

Porous material

Model

solid matrix
air and water vapour
liquid water

low moisture content,
dominating vapour diffusion

mean moisture content

high moisture content
dominating liquid water flux

serial   parallel
liquid water and vapour
transport
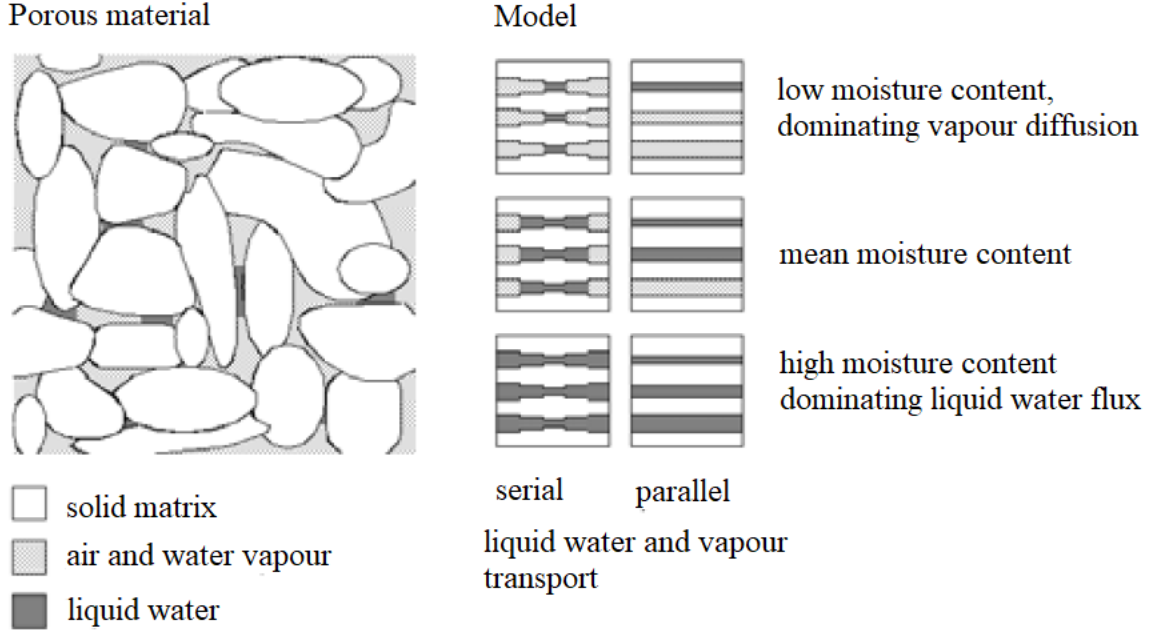
Figure 6: Visual explanation of the difference between serial and parallel domains (Grunewald, John; Häupl, Peter; Bomberg, 2003)

If the following assumptions are made:

- No air transfer, no thermal gradient driven liquid transfer, no effect of gravity
- No radiative transfer, no exceeding of the boiling temperature of water, and
- No contribution of the vapour phase on moisture nor heat storage

The moisture and vapour transport can be expressed as (Janssen, Blocken and Carmeliet, 2007):

$$\frac{\partial \varepsilon}{\partial t} = -C_{Pc}\frac{\partial P_c}{\partial t}$$

Eq.8

Where: C_{Pc} is the moisture capacity at the given capillary pressure P_c.

The dependency on the different parameters regarding the liquid and vapour phase can further be described by Eq.9:

$$-C_{Pc}\frac{\partial P_c}{\partial t} = -\nabla(\frac{D_v(\Theta_l)}{R\,T}\frac{P_v, sat\ \varphi}{\rho_l\,R\,T} + K_l(\Theta_l)\nabla P_c)$$

Eq.9

The two main transport coefficients are the vapour diffusion coefficient D_v and the liquid conductivity K_l those coefficients are given as function of the moisture content.

As the used conductivity model simplifies the pore structure to tubes, a scaling factor is introduced. This scaling factor depends on the moisture content and the number of parallel tube

domains and therefore refers to the mechanistic approach presented. The scaling factor f for the liquid and vapour phase as presented in (Scheffler and Plagge, 2010) is calculated as:

$$f_{(l,v)} = [\frac{p}{p + (1 - \Theta)^2 (1 - p)}]$$

Eq.10

Where Θ is the relative moisture content and p is a term for increasing domains allowing for parallel moisture transport in the pores due to increasing moisture content:

$$p = p(\Theta, \eta_{sp}) = \Theta^{\eta_{sp}}$$

Eq.11

η_{sp} is a parameter to account for the parallel pore domains as function of the relative moisture content M.

The relative moisture content is calculated as the volume ratio of moisture content and porosity

$$\Theta = \frac{\theta_l}{\theta_{por}}$$

Eq.12

Substituting Eq.10 with the terms for Θ and p leads to following two scaling factors for the liquid and vapour phase respectively (Michel *et al.*, 2019):

$$f_v = \frac{1 - \frac{\theta_l}{\theta_{por}}}{\left(\frac{\theta_l}{\theta_{por}}\right)^{\eta_{sp}} + \left(1 - \frac{\theta_l}{\theta_{por}}\right)^2 + (1 - \left(\frac{\theta_l}{\theta_{por}}\right)^{\eta_{sp}})}$$

Eq.13

$$f_l = \frac{\left(\frac{\theta_l}{\theta_{por}}\right)^{\eta_{sp}}}{\left(\frac{\theta_l}{\theta_{por}}\right)^{\eta_{sp}} + \left(1 - \frac{\theta_l}{\theta_{por}}\right)^2 + (1 - \left(\frac{\theta_l}{\theta_{por}}\right)^{\eta_{sp}})}$$

Eq.14

As shown by (Schirmer, 1938) the Diffusion coefficient for air can be described as:

$$D_{v,air} = 0.083 \frac{P_0}{P} \left(\frac{T}{273.15}\right)^{1.81}$$

Eq.15

In this formula P_0 is the reference pressure of 101,323 Pa and P the ambient air pressure. By dividing the $D_{v,air}$ value by an experimentally determined diffusion resistance number µ, which is a specific and easy determinable material parameter, the material vapour permeability can be

calculated. Up or downscaling with the introduced scaling factor f_v leads to following equation (Scheffler and Plagge, 2010):

$$D_v(\Theta_l) = \frac{D_{v,air}}{\mu_{dry}} f_v(\Theta_l)$$

Eq.16

The relative liquid conductivity is calculated by :

$$K_{l,rel}(\Theta_l) = \left(\frac{\int_0^{\theta_l} P_c(\theta)^{-2} d\theta}{\int_0^{\theta_{sat}} P_c(\theta)^{-2} d\theta} \right)$$

Eq.17

To account for the overestimated conductivity and consider the mechanistic approach the liquid phase scaling factor f_l is applied:

$$K_l(\Theta_l) = K_{l,rel}(\Theta) f_l(\Theta) K_{l,sat}$$

Eq.18

It is important to mention at this point that this part of the model is only intended to model the moisture transport. The scaling factor presented accounts for the moisture content only and the hereby calculated connectivity is not applied to the ionic transport itself.

2.2.4. Description of model input

The model framework offers the usage of a variety of input parameters, which have to be chosen carefully. As the model code is written as a MATLAB-code an excel sheet has been developed by Victor Meson (DTU BYG), to have a simplified and more structured overview on the input. The Matlab code extracts the input parameters from the excel sheet. The input can be diverted in six main classes:

1. Spatial
2. Time
3. Binder
4. Multi-phase transport
5. Chemical
6. Physics
7. Miscellaneous

2.2.4.1. Spatial

The spatial parameters describe the space of the modelled system. Inputs are the length $[m]$ of the simulated system in one dimensional direction, the number of elements $[-]$ along the given length and the element cross-sectional setup in the one-dimensional system $[m^2]$. The area of interest $[m]$ can be modified if needed, this reduces the resolution outside the chosen area and therefore lowers the required computational power. This is especially useful if a certain area of a sample should be investigated. If for example a total length of one meter is chosen and ten elements are defined, an area of interest of 0.1 meter would mean that all ten elements are spaced in this first 0.1 meter followed by a large single element of 0.9 meters. A growth factor $[-]$ defines the position of the nodes between the different elements and describes the relation between element one and element number x. A growth factor of one means equally spaced elements, a growth factor below one results in a finer mesh further away from the boundary and a value of bigger than one will result in a higher resolution next to the boundary.

2.2.4.2. Time

The time parameter allows for optimization of the stepwise numerical calculation. The total calculation time $[h]$ sets the boundary for the step sizes $[h]$. If the step size is e.g. set to one hour and the total calculation time to 24 hours, there will be 24 time steps. The interval of the chemical equilibrium $[h]$ calculation can be set according to the needs. This input in general determines how often the chemical equilibrium will be solved over the total time. In general, it is a rather complex solution process based on the PHREEQC code and therefore requires computational power increasing the overall runtime. Uncoupling it from the general step size allows to decrease the total runtime but influences the accuracy and outcome of the model. An acceleration factor [-] related to the FEM transport scheme allows to influence step sizes related to transport parameters. In reactive mass transport modelling stability of the code and computational speed are of major importance. A thorough discussion on that matter can be found in (Jensen, 2014).

2.2.4.3. Binder

The binder system can be separated into three sub sections. The subsections determine the binder composition, the hydration process and in the case of a concrete mixture the considered mix proportions.

In the binder composition the following oxides are considered in terms of mass percentage and are required input parameters $[wt.\%]$:

$$CaO, SiO_2, Al_2O_3, Fe_2O_3, SO_3, K_2O, Na_2O, MgO, CaSO_4, CO_2$$
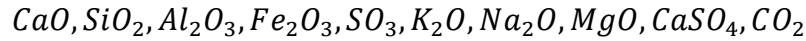
Also the initial Cl content $[wt.\%]$ is one input parameter in this step.

The hydration is based on the maturity concept and for the hydration law two main maturity parameters are crucial, a shape factor $[-]$ and reaction rate factor $[-]$. Other input here is the calibrated activation energy of the binder $[\frac{J}{mol}]$, the reference temperature $[K]$, the curing time $[days]$ and the reference maturity $[days]$. In the mix design, general mixing parameters such as the w/c ratio $[-]$ and entrained air porosity $[\frac{m^3}{m^3}]$ are defined. Here it is also decided if a concrete or cement paste will be simulated by defining a total aggregate volume ratio $[\frac{m^3}{m^3}]$ and setting the density of the assumingly inert aggregate phase $[\frac{g}{cm^3}]$. The code also requires a reference volume, typically $1 \left[\frac{m^3}{m^3}\right]$, to calculate the mentioned ratios.

2.2.4.4. Multi-phase transport

This section includes parameters needed to describe the pore structure and general transport in the system.

The pore structure and pore size distribution (PSD) is based on classification into gel, capillary and macro pores. An initial total pore area $[\frac{m^2}{m^3}]$, which is dependent on the pore volume, has to be set. The mean pore radii $[\mu m]$ determines the differentiation between the three pore types, therefore three input values are required. The pore radii standard deviation $[-]$ describes the spread of the pores. The distribution of pore volume change $[\%]$ ascribed to the gel, capillary or macro porosity has to be set. Here again three values are needed where an input of e.g. $[0.7, 0.25, 0.05]$ means that 70% of pore volume change will be attributed to gel pores, 25% to capillary pores and 5% to macro pores. The contact angle of water $[degrees]$ and the surfaces tension $[\frac{N}{m}]$ are two other important values for pore size distribution determination. It is important to mention that the contact angle differs for adsorption and desorption, therefore two input values are required. The volume to area ratio $[\frac{m^2}{m^3}]$ of the pores is derived from the calculated PSD. The reaction depth $[m]$ defines the volume of solids, which is available for reaction with the pore solution. The default input, 0, allows reaction of all solids.

For the connectivity of the pore system, ionic transport and moisture/gas transport have to be distinguished. In Section 2.2.3 a scaling factor has been introduced. This scaling factor requires input of serial and parallel connectivity $[-]$ a global liquid connectivity $[-]$, the dry vapour

diffusion resistance number $[-]$ as well as the effective moisture conductivity at saturation $[S]$. As earlier explained, this is only applied for moisture and gas transport where the gas-liquid interactions are handled by the chemical solver function. For ionic transport the connectivity is described in terms of a more common tortuosity function requiring input of a tortuosity factor $[-]$, tortuosity shape $[-]$ and tortuosity limit $[-]$ to define the function. The advective transport stream upwinding coefficient $[-]$ is needed for appropriate consideration of advective ion transport and balances between advective and diffusive processes. The initial moisture flux (input 1 or 0) describes the flux direction, meaning at the start of the simulation with adsorption or desorption.

2.2.4.5. Chemical

As mentioned before the chemical solver is based on PHREEQC in connection to the Cemdata18 database (Lothenbach *et al.*, 2019). This allows for consideration of 80 different ions and 138 different phase equilibria (considered species found in table A7 in the appendices) with a simple 0/1 statement, the different equilibrium reactions and ions can be considered or excluded in the solver. In this part of the parameter selection, the most computational power and time can be saved by appropriate selection of necessary species for the performed simulation. It is also possible to set a boundary pressure $[Pa]$, determining the relative humidity at the given boundary and imposed current $[C]$ on the boundary. Where most of the times both might be omitted. Meaning no external oppressed force on the system is interfering.

2.2.4.6. Physics

The user can decide which physics should be included in the calculation. With a true or false (T/F) statement following physics can be turned on or off: The ionic transport due to diffusion; The ionic transport due to electromigration; Moisture transport, which if activated automatically includes the advection; Hysteresis which with every step recalculates hysteretic behaviour; Recalculation of the PSD, which means the pore radius and pore volume; Inclusion or exclusion of the Chemical equilibrium solver and the water balance, meaning the self-ionization of the water during transport for each step; In addition to this, it is possible to activate a Newton-Raphson optimization scheme, which requires some additional input boundaries for the scheme itself.

2.2.4.7. Miscellaneous

Saving intervals $[h]$ and plotting intervals $[h]$ can be selected and turned either on or off to save and plot the result. Some basic constants such as exposure temperature of the system during

simulation $[K]$, the solution density $[\frac{kg}{m^3}]$ e.g. 1000 for pure water and Dielectricity in the chosen solution and vacuum $[\frac{F}{m}]$ have to be selected. A maximum number of iteration steps as well as some error tolerances can be added to the simulation.

Including the chemical phases and input parameters to the general setup options the presented model requires some 306 input statements. This highlights the importance of careful assumptions and selection as most of those statements interact with each other. This huge variety offers simulation of more realistic cement binder systems with the possibility of defining very detailed and carefully selected exposure and material conditions.

2.3. Modelling methodology of chloride binding

There are different methods to predict chloride binding and consequently ingress in cementitious materials. In their comprehensive study Baroghel-Bouny et al. focus on prediction of chloride binding isotherms and separated the prediction by modelling into two main groups with different approaches (Baroghel-bouny *et al.*, 2012).

1. Prediction-based on a model using numerical inverse analysis from experimental data
2. Prediction-based on an analytical model using material composition

The first group consists of a total chloride content profile, which is obtained by laboratory experiments and calculated back to a binding isotherm. A one-dimensional multispecies ion transport model considering ion flux by combining a diffusion coefficient with electro-migration by means of the Nernst-Planck equation is used. The chloride profile calculated by the model is fit to the profile determined by experimental work. In the simple variant such a model assumes isothermal and saturated conditions and only considers specific ions in the pore solution that are classified as significant as for example shown in a paper by Nguyen, Baroghel-Bouny and Dangla (Nguyen, Baroghel-Bouny and Dangla, 2006). The diffusion coefficient used in this model is dependent on porosity and tortuosity of the system. A simplified model build up in this way requires the effective chloride diffusion coefficient. As chlorides are only transported in solution, the effective chloride diffusion coefficient is dependent on the porosity accessible to water as well as the tortuosity of the pore system. Parameters describing the chloride binding isotherm of the Freundlich form ($S_{Cl} = \mu * C_{Cl}^{\Upsilon}$) and the composition of the pore solution are also necessary. The binding parameters Υ and μ are adjusted by a numerical algorithm until a good agreement between experimental and calculated data is reached.

The second group can be used for a material at a specific age. The proposed procedure includes differentiation between chemical chloride binding and physical chloride binding. In Baroghel's approach chemical binding is considered to occur instant through Friedel's salt formation at low chloride concentrations when the material first gets in contact with chlorides as proposed by e.g. Nilsson et al. (Nilsson *et al.*, 1996). The initial chemical binding is therefore only dependent on the equivalent aluminate content. The equivalent aluminate content is a simplification allowing to relate both C_3A and C_4AF phases to Friedel's salt formation. This simplification accounts double the contribution of C_3A compared to the one of C_4AF to the Friedel's salt formation.

With the assumption that Friedel's salt is formed at low chloride concentrations and instantly the chemical binding becomes unrelated to the chloride concentration and only related to the equivalent aluminate content representing it at the ordinate of X=0. However, the physical binding is considered as a function dependent on the C-S-H content of the material and the chloride concentration. To assess the amount of equivalent aluminate content and the C-S-H content a hydration model is required. (Baroghel-bouny *et al.*, 2012) use an analytical approach as presented by Mounaga et al. that depends on the cement composition, a set of governing chemical reactions that are considered in formation of the chemical phases during the hydration process and the degree of hydration of the resulting phase based on the age (Mounanga *et al.*, 2004). Even though this approach is based on kinetics it is simplified and only validated for the assessment of C-S-H content in CEM 1 materials(Baroghel-Bouny, 2007).

In the model the physical binding is included by an isotherm description of

    a. The Freundlich form

    b. The Langmuir form $S_{Cl\,physical} = N_{CSH} * \frac{\alpha * C_{cl}}{1 + \beta * C_{Cl}}$

    c. The modified Langmuir form $S_{Cl\,physical} = N_{CSH} * \frac{\alpha * C_{cl}}{C_{OH} + \beta * C_{Cl}}$

The form of a generalized and simplified combined chloride binding isotherm assuming the instantaneous Friedel's salt formation and physical adsorption then has the form shown in Figure 7.

As shown both groups of prediction techniques are addressed with different methods, Baroghel et al. showed that there exists good agreement between the proposed methods and experimental data (Baroghel-bouny *et al.*, 2012). However, a drawback is the requirement of laboratory

testing and its results to predict chloride binding isotherms which can then be used in modelling for prediction of ingress.
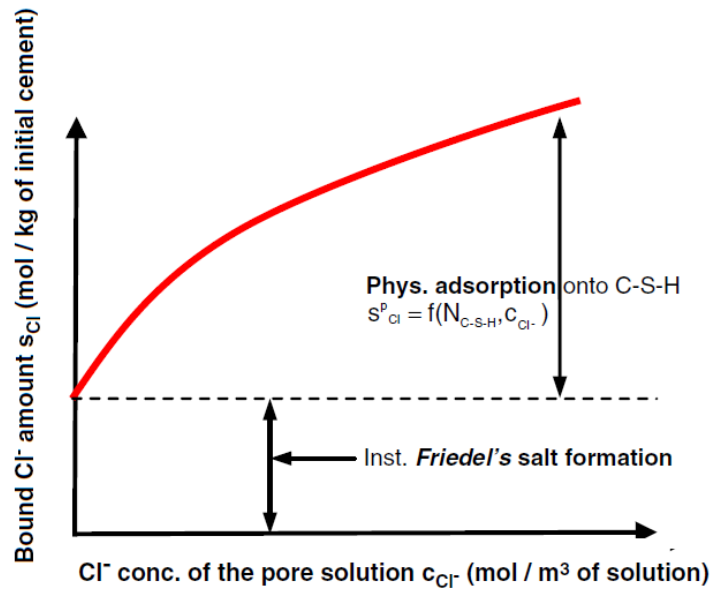
Figure 7: Generalized, simplified form of chloride binding isotherm (Baroghel-bouny *et al.*, 2012)

Another way to tackle the problem of chloride binding is simulation of the material composition. Phase assemblage and changes in the phase assemblage of the material can be modelled using different software considering thermodynamic properties. Two examples for those software are the Gibbs Free Energy Minimization Software GEMS (Kulik *et al.*, 2015) or PHREEQC (Parkhurst and Appelo, 2013). As those software are not specifically build for applications regarding cement hydration or chloride binding in cementitious systems they need supplementation of thermodynamic data relevant for those applications. Various publications with big contribution of the Swiss Federal Laboratories for Materials Science and Technology (EMPA) aim to provide useable cement related data as for example in (Lothenbach and Winnefeld, 2006; Matschei, Lothenbach and Glasser, 2007; Lothenbach *et al.*, 2008; Balonis *et al.*, 2010; Dilnesa *et al.*, 2011). The scientific database CEMDATA combines relevant thermodynamic data for cementitious materials. It is frequently updated and in its current version CEMDATA 18 freely available (Lothenbach *et al.*, 2019). To utilize the thermodynamic data a model with a clear structural and mechanistic basis such as the C-S-H solid solution model proposed by Kulik can be applied (Kulik, 2011). Studies that make use of either PHREEQC or GEMS for thermodynamic modelling and/or comparison to experimental

data include for example (Hosokawa *et al.*, 2006; Pointeau *et al.*, 2006; yoga *et al.*, 2010; Thiéry and Wang, 2011; Jensen *et al.*, 2015; Weerdt *et al.*, 2015; Shi, Geiker, De Weerdt, *et al.*, 2017b; Shi, Geiker, Lothenbach, *et al.*, 2017b; Hemstad, Machner and De Weerdt, 2020). In general those studies show a good agreement between data of phase assemblage and chemical chloride binding (e.g. in Friedel's salt) which has been calculated and the one observed by measurements, making thermodynamic modelling a powerful tool. Combining the phase assemblage from thermodynamic considerations with other modelling approaches for transport and material parameters can be used to extend the possibilities and not only predict binding properties at a given time but also for example at a given point in space and lead to a chloride ingress profile as has been done in the introduced model framework in Section 2.2. Modelling requires the initial composition and conditions but there is no need of experimental data (using the CEM database) to predict the phase assemblage itself. Thus, the chloride chemically bound in Friedel's salt can be predicted for any cementitious material with a given composition, exposure and age. However, the pure thermodynamic character is a drawback in terms of the physically bound chloride. As it does not appear directly bound in one of the hydrate phases it cannot be calculated itself by thermodynamic considerations. Surface complexation and electrostatics, which have been introduced in Section 2.1.1 are therefore not considered in the calculations.

2.3.1. Incorporation of physical bound chloride

There are two approaches that should be discussed to include the physical binding into a model based on thermodynamics.

2.3.1.1. Simple inclusion

A simple way would be a combination of a thermodynamic model and addition of chloride bound physically to the chemically bound chloride in the Friedel's salt. By use of one of the functions (Freundlich, Langmuir, modified Langmuir) as proposed in the model group 2 by Baroghel et al.. This can be done after calibration of data on physical binding from experimental work (Baroghel-bouny *et al.*, 2012).

2.3.1.2. Complex inclusion

The other more complex method includes the modelling of surface complexation with charge considerations, which has been introduced in Section 2.1.1. The modelling approach presented in (Yogarajah, Nawa and Kurumisawa, 2018) uses the geochemical code PHREEQC. Built-in modelling approaches and thermodynamic datasets as well as an extension with the

CEMDATA07 database has been used for their calculations. The PHREEQC software includes two possible surface complexation models. One model is based on the model described by Dzombak and Morel (Dzombak and Morel, 1990). This model makes use of the Gouy-Chapman theory and equation to consider electrostatic interactions of surfaces and adsorbates. Another model is the charge distribution multisite complexation model (short CD-MUSIC) which offers a few more options than the model by Dzombak and Morel (Hiemstra and Van Riemsdijk, 1996). In both cases, the surface charge is neutralized by an electrical double layer. Yogarajah et al. use the model proposed by Dzombak and Morel in connection with other further on explained approaches to calculate the surface site density, dissociation of the surface sites and finally the adsorption of different ionic species.

Following assumptions are made (Yogarajah, Nawa and Kurumisawa, 2018):

- All surface complexes are assumed to be inner-sphere complexes meaning that ions bind directly to the surface without intervening water molecules that formerly formed a water-surface interface.
- Electrolyte background ions are indifferent ions that adsorb through Coulomb forces only and are not adsorbed on an uncharged surface.
- The C-S-H surface consists only of one type of surface sites, silanol sites ($SiOH$)

To determine the surface electrical properties of C-S-H, Vogarajah et al. use an approach as proposed in (Mayant *et al.*, 2008). In this approach the surface charge density ($\sigma_{exposed}$) $[\frac{C}{m^2}]$ is determined from the difference in the total and the free hydroxyl concentration.

$$\sigma_{exp} = \frac{F}{A \cdot S} \left(\frac{-[NaOH] \cdot V_{NaOH,add} - \{[OH^-]_{init} - [H^+]_{init}\} \cdot V_{init}}{V_{init} + V_{NaOH,add}} + [OH^-]_{fin} - [H^+]_{fin} \right) \qquad \text{Eq.19}$$

With F is the Faraday constant $\left[\frac{C}{m^2}\right]$, A is the specific surface area $\left[\frac{g}{m^2}\right]$, S is the solid concentration $\left[\frac{g}{l}\right]$, $V_{NaOH,add}$ and V_{init} are volumes of added NaOH and initial $NaNO_3$ salt which was used in a tritration experiment to maintain a constant ionic strength. [NaOH] is the molar concentration of the titrant, $[OH^-]_{init}, [OH^-]_{fin}, [H^+]_{init}, [H^+]_{fin}$ are molar concentrations of OH^- and H^+ derived from the pH of initial and final solution.

The main mechanism that is considered to cause surface charge on the C-S-H surface is the deprotonation (see Section 2.1.1) (Helene Viallis-Terrisse, Andre Nonat, 2001; Elakneswaran, Nawa and Kurumisawa, 2009):

$$\equiv \text{SiOH} + \text{OH}^- \Longleftrightarrow \equiv \text{SiO}^- + \text{H}_2\text{O}$$
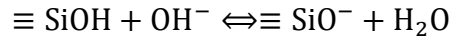
The intrinsic equilibrium constant can be calculated as

$$\text{K}_{\text{OH}} = \frac{a_{SiO^-}}{a_{SiOH} \cdot a_{OH^-}} \exp\left(-\frac{F\Psi_o}{RT}\right) \qquad \text{Eq.20}$$

Where K_{OH} is the intrinsic equilibrium constant for deprotonation, a is the activity of the species, Ψ_o is the surface potential $[V]$, R is the universal gas constant and T is the temperature [k].

To include charge reversal due to overcharging the related reaction should as well be considered by an equilibrium constant (Helene Viallis-Terrisse, Andre Nonat, 2001; Elakneswaran, Nawa and Kurumisawa, 2009):

$$\equiv SiOH + Ca^{2+} \Longleftrightarrow \equiv SiOCa^{2+} + H^+$$

$$K_{Ca} = \frac{a_{SiOCa^+} \cdot a_{H^+}}{a_{SiOH} \cdot a_{Ca^{2+}}} \exp\left(\frac{F\Psi_o}{RT}\right) \qquad \text{Eq.21}$$

Surface charge density $\sigma \left[\frac{\text{C}}{\text{m}^2}\right]$ is changed by the dissociation as well as the complexation processes and can be expressed by:

$$\sigma = \frac{F}{AS}[(\equiv \text{SiOCa}^+) - (\equiv \text{SiO}^-)]$$

$(\equiv \text{SiOCa}^+)$ and $(\equiv \text{SiO}^-)$ express the the concentrations of the two different surface species in $\left[\frac{\text{mol}}{\text{l}}\right]$.

To relate the charge σ to surface potential the gouy chapman theory is used:

$$\sigma = (8000\varepsilon\varepsilon_0 \text{RT}\mu)^{1/2} \sinh\left(\frac{ZF\Psi_o}{RT}\right) \qquad \text{Eq.22}$$

With ε is the dielectric constant of water, ε_0 is the permittivity of free space $\left[\frac{\text{C}}{\text{V}\cdot\text{m}}\right]$ and μ is the ionic strength.

(Yogarajah, Nawa and Kurumisawa, 2018) use the presented approach and fit it to experimental data to calculate the constants K_{OH} and K_{Ca}. Surface site density is obtained by fitting experimental data from a titration experiment to data obtained by Eq.19.

To include highly charged C-S-H, where chloride even adsorbs to calcium adsorbed surfaces an additional equilibrium constant is included:

$$\equiv SiOH + Ca^{2+} + Cl^- \Leftrightarrow \equiv SiOCaCl + H^+$$
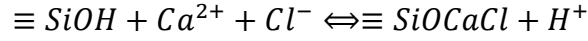
$$K_{CaCL} = \frac{a_{SiOCaCl} \cdot a_{H^+}}{a_{SiOH} \cdot a_{Ca^{2+}} \cdot a_{Cl^-}} \exp\left(\frac{ZF\Psi_o}{RT}\right) \qquad \text{Eq.23}$$

In fact there are different proposed values and good accuracy depends on appropriate and careful selection.

Heath and Ilett calculated values for pure silica surfaces and pure calcium hydroxide surfaces based on a literature review as well as fitting some experimental data of zeta potential studies. Log K has been calculated assuming that it varies linearly with the mole fraction of calcium surface sites $X_s(Ca)$.

Table 1: log K for C-S-H surface reactions (Heath, T. G., D. J. Ilett, 1996)

complexation reaction	$X_s(Ca) = 0$	$X_s(Ca) = 1$
$\equiv SiOH + H^+ \Leftrightarrow \equiv SiOH_2^+$	-2.8	-2.8
$\equiv SiOH \Leftrightarrow \equiv SiO^- + H^+$	-6.8	-6.8
$\equiv SiOH + Ca^{2+} + H_2O \Leftrightarrow \equiv SiOCaOH + 2H^+$	-17	-15.1
$\equiv SiOCaOH + H^+ \Leftrightarrow \equiv SiOCaOH_2^+$	8.3	12.6
$\equiv SiCaOH \Leftrightarrow \equiv SiOCaO^- + H^+$	-13.4	-13.4

Viallis-Terrisse and Nonat assume that only the two reactions of silanol deprotonation and calcium sorption are reactions of major importance and dominate the surface chemistry of C-S-H (Table 2).

Also Pointeau et al. assume that the surface chemistry is dominated by those two surface reactions and showed by acid titration that the values of (Helene Viallis-Terrisse, Andre Nonat, 2001) are in good agreement with experimental work (Table 3):

Hosokawa et al. derive values with PHREEQC by calibrating against experimental sorption data. Values for silanol deprotonation and calcium complexation by (Helene Viallis-Terrisse, Andre Nonat, 2001) are considered in their calculated values (Table 4).

Table 2: log K for C-S-H surface reactions (Helene Viallis-Terrisse, Andre Nonat, 2001)

Ca/Si ratio of C-S-H = 1.5	
complexation reaction	log K
$\equiv SiOH \Leftrightarrow \equiv SiO^- + H^+$	-12.3
$\equiv SiOH + Ca^{2+} \Leftrightarrow \equiv SiOCa^+ + H^+$	-9.4

Table 3: log K values for C-S-H surface reactions (Pointeau et al., 2006)

complexation reaction	Ca/Si ratio of C-S-H Not specified log K
$\equiv SiOH \Leftrightarrow \equiv SiO^- + H^+$	-12.0
$\equiv SiOH + Ca^{2+} \Leftrightarrow \equiv SiOCa^+ + H^+$	-9.2

Table 4: log K values for C-S-H surface reactions (Hosokawa et al., 2006)

complexation reaction	Ca/Si ratio of C-S-H				
	0.85	1.2	1.5	1.75	1.45
	log K				
$\equiv SiOH + Na^+ \Leftrightarrow \equiv SiONa + H^+$	-11.1	-11.4	-11.7	-11.7	-
$\equiv SiOH + K^+ \Leftrightarrow \equiv SiOK + H^+$	-11.3	-11.6	-11.6	-11.6	-
$\equiv SiOH + Ca^{2+} + Cl^- \Leftrightarrow \equiv SiOCaCl + H^+$					-8.9
$\equiv SiOH + Ca^{2+} + SO_4^{2-} \Leftrightarrow \equiv SiOCaSO_4^- + H^+$					-6.0

3. Experimental data

3.1. Experimental work and data

Following the experimental work by (Shi, Geiker, De Weerdt, *et al.*, 2017b) and the way results were received shall be explained. Table 5 summarizes the experimental work and execution. A more detailed summary, including compositions and important results follows. A thorough description including additional measurements that are not directly connected to the matter of interest are available within the cited source.

Table 5: Summary of experimental work

Source	(Shi, Geiker, De Weerdt, *et al.*, 2017b)
Material	1) "P" pure wPc binder (white Portland cement); 2) "ML" wPc with metakaolin and limestone substitution; 3) "M" wPc with metakaolin substitution
w/b	0.5/0.95
Curing conditions	three days at 5°C sealed, two months in moist room RH >98% at 20°C after initial curing samples crushed and powders mixed with distilled water to reach w/b 0.95 -> rotation cured for 7 days; following ball mill crushing
pore solution extraction	Centrifugation of samples
exposure	equilibrium concentration technique; 30g sample in 15ml of 1) NaCl and 2) CaCl2 solution, sealed, stored for two months, initial chloride concentrations 0, 0.125, 0.25, 0.5, 1.0, 2.0 mol/l
analysis	total bound chlorides determined from initial and equilibrium concentration after exposure; XRD and TGA to determine Friedel's salt; chloride concentrations of extracted pore liquid measured by potentiometric titration; thermodynamic modelling with GEMS to calculate initial phase assemblage as well as phase assemblage under exposure conditions

In this study three different binder were produced from white Portland cement (wPc), metakaolin (MK) and limestone (LM), always maintaining an initial w/b ratio of 0.5. The composition of the different starting materials is shown in Table 6. The three different pastes were obtained by mixing the materials according to the binder compositions shown in Table 7:

Table 6: Chemical composition of starting materials (wt.%), LOI, density and blaine fineness (Shi, Geiker, De Weerdt, *et al.*, 2017b)

	wPc	LS	MK
CaO	66.13	53.73	0.22
SiO2	21.81	3.92	52.84
Al2O3	3.56	0.33	39.49
Fe2O3	0.24	0.14	1.42
SO3	3.37	0.05	0.06
K2O	0.43	0.05	1
Na2O	0.04	0.08	0.05
MgO	1.1	0.35	0.48
TiO2	0.21	0.02	0.88
P2O5	0.04	0.1	0.11
LOI	2.57	41.8	3.55
Density (kg/m3)	3080	2700	2530
Blaine fineness m2/kg)	387	1211	1891
carbon content	0.37	-	-
CaCO3	3.1	93.8	-

Table 7: Binder compositions (wt.%) (Shi, Geiker, De Weerdt, *et al.*, 2017b)

Material index	wPc	MK	LS
P	100	-	-
ML	68.1	25.5	6.4
M	68.1	31.9	-

Table 8: Phase composition wPc by SI MAS NMR *(Shi, Geiker, De Weerdt,* et al*., 2017b)*

Phase	Wt.%
alite ("3CaO·SiO2": C3S)	64.9
belite ("2CaO·SiO2": C2S)	16.9
calcium aluminate (3CaO·Al2O3: C3A)	7.8

Table 9: Degree of hydration of alite, belite and metakaolin after 28 and 180 days of hydration (Shi, Geiker, De Weerdt, *et al.*, 2017b)

	28d	180d	28d	180d	28d	180d
Blend	Alite		Belite		MK	
P	81	95	25	63	-	-
ML	83	86	34	36	48	54
M	86	86	34	34	38	50

The phase composition of the wPc was determined by Shi et al. with Si MAS NMR as described in (Poulsen *et al.*, 2009) to have the composition shown in Table 8. Si MAS NMR is also used to determine the degree of hydration of Alite, Belite and Metakaolin (Table 9).

The paste samples, produced in accordance to Table 7, were sealed cured at 5°C Celsius for three days and afterwards stored in a moist room for two months at 20°C. After curing samples were crushed to a size of approximately 1mm. Crushed samples were collected and mixed with 30% by mass of crushed paste with distilled water (resulting in w/b 0.95) and rotation cured for 7 days at 20°C. After rotation curing samples were crushed with a ball mill. In this way Shi et al. assumed that samples reach a maximized DOH and the possibility of carbonation is reduced. Chloride binding isotherms were obtained by the equilibrium approach. 30g of sample were exposed to 15ml chloride solution in centrifuge tubes at 20°C for two months. The chloride ion concentrations of the exposure solutions were 0, 0.125, 0.25, 0.50, 1.0 and 2.0 mol/L. $CaCl_2$ as well as $NaCl$ salt of laboratory grade was used to produce those solutions. The chloride content of the samples after two months of exposure was measured by Thermogravimetric analysis (TGA) and XRD.

The samples in the tubes were centrifuged after two months chloride exposure. It is assumed that the centrifuged solution shows the same chloride concentration as the pore solution, even though Shi et al. acknowledged that centrifugation would not completely remove the pore solution from the samples. Chloride concentrations of the extracted solutions were determined by potentiometric titration.

The total chloride content was concluded from the difference in measured equilibrium chloride concentration and initial chloride concentration (found in table A2 in the Appendix) and reported in $g/g\ unhydrated\ cement$. The author assumes that chemical binding is dominated by Friedel's salt formation and physical binding by adsorption of chlorides onto C-S-H. The amount of Friedel's salt is investigated by experimental analysis (TGA/XRD) and thermodynamic modelling, showing a good agreement between those measurements and modelled results.

3.2. Treatment and usage of data

To assess the amount of physical bound chloride, certain data is required. The following section explains which data was used from (Shi, Geiker, De Weerdt, *et al.*, 2017b) and how it was treated to receive the amount of physical bound chloride.

The amount of physical bound chloride is calculated as the difference between chloride bound in Friedel's salt (FS) and total bound chloride. Minor amounts of chloride may also be chemical bound in other phases than Friedel's but are assumed to be neglectable.

$$C_{Cl,physical} = C_{Cl,total} - C_{Cl,FS} \qquad \text{Eq.24}$$

As mentioned in Section 3.1 the amount of chloride bound in Friedel's salt can be determined in different ways. For example, by thermodynamic modelling or experimental TGA and XRD measurements. The amount of total chloride is calculated by Eq.25:

$$C_{Cl,total}\left[\frac{g}{g\ paste}\right] = \frac{M_{Cl} * \left(C_{Cl,free,0} - C_{Cl,eq.}\right) * \left(V_{Cl,added} + V_{H_2O,free}\right)/1000}{\dfrac{m_{sample}}{w/b}} \qquad \text{Eq.25}$$

With M_{Cl} being the molar mass of Cl, $M_{Cl} = 35,45\left[\frac{g}{mol}\right]$, $C_{Cl,eq.}$ is the equilibrium concentration of chlorides in the final solution $[\frac{mol}{l}]$ and m_{sample} is the wet sample mass in $[g]$. The amount of free initial chloride, $C_{Cl,free,0}$, is calculated by:

$$C_{Cl,free,0}\left[\frac{mol}{l}\right] = \frac{V_{Cl,added} * C_{cl,added}}{V_{Cl,added} + V_{H_2O,free}} \qquad \text{Eq.26}$$

With V_{H_2O} being the free water of the sample obtained by $V_{H_2O} = \frac{mass\ of\ sample * wt.\%\ free\ water}{100}$ [ml], $V_{Cl,added}$ is the volume of added exposure solution in [ml] and $C_{cl,added}$ is the concentration of added chloride in the exposure solution [$\frac{mol}{l}$].

The amount of Friedel's salt and total bound chloride of the equilibrated samples can be found in the Appendix in table A3 and table A4. After calculation of the physical bound chlorides as shown in Eq.24, the amount of physical bound chloride ($C_{Cl,physical}$) is fit to a modified Langmuir isotherm expression as has been introduced in in Section 2.1.1 and used by e.g. (Ye *et al.*, 2016) or (Baroghel-bouny *et al.*, 2012) with the form of Eq.27:

$$C_{Cl\ physical} = x * \frac{\alpha * C_{cl}}{1 + \beta * C_{Cl}} \qquad \text{Eq.27}$$

Where x is the scaling factor, α is the binding parameter α and β is the binding parameter β.

To fit the modified langmuir expression the excel built in solver function is used to find the least root mean square error.

To asses the impact of physical binding the initial phase assemblage and change with chloride exposure as well as the amount of bound chlorides (physical, chemical) has to be investigated. For this matter initial phase assemblage calculations are compared to calculations by Shi et al.. After matching a comparable trend physical binding is included:

1. before the chemical solver is run
2. after the chemical solver is run

The used input format via an excel sheet for the model requires input of the chemical compositions for the different materials. The chemical composition has to contain information about the content of CaO, SiO_2, Al_2O_3, Fe_2O_3, SO_3, K_2O, Na_2O, MgO, $CaSO_4$, $NaCl$ and CO_2 as has already been introduced in Section 2.2.

Combination of the data from Shi et al. as presented in Table 6 and Table 7 gives the combined composition used as input value for the different materials (Table 10):

Table 10: Combined chemical composition of the different mixtures for thermodynamic modelling (wt.%)

	P	**ML**	**M**
CaO	66.13	48.53	45.10
SiO2	21.81	28.58	31.71
Al2O3	3.56	12.52	15.02
Fe2O3	0.24	0.53	0.62
SO3	3.37	2.31	2.31
K2O	0.43	0.55	0.61
Na2O	0.04	0.05	0.04
MgO	1.1	0.89	0.90
CaSO4	4.1	2.79	2.79
NaCl	-	-	-
CO2	-	-	-

In addition to the chemical composition, the degree of reactivity for the different components has to be defined. Shi et al. provided the degree of hydration for Alite, Belite and Metakaolin for 28 and 180 days, dependent on the mix, as shown in Table 9. To get an idea about the degree of hydration and reactivity of the combined materials the different oxides originating from the mentioned phases can be combined in accordance to assumed phase composition (Table 11) and the individual degree of hydration.

Table 11: Assumed chemical phase composition Alite, Belite, Tricalcium aluminate and Metakaolin

Alite Ca_3SiO_5		Belite Ca_2SiO_4		C3A $3CaOAl_2O_3$		Metakaolin $Al_2Si_2O_7$	
Oxides	wt.%	Oxides	wt.%	Oxides	wt.%	Oxides	wt.%
SiO2	26.31	SiO2	34.884	Al2O3	37.736	Al2O3	45.902
CaO	73.69	CaO	65.116	CaO	62.264	SiO2	54.098

With this assumptions and Data given for 180 days of hydration the initial model input for reactivity combines to the values shown in table A7 in the appendix. However, this combination is at its best valid for samples at the age of 180 days of hydration. Shi et al. exposed the samples in their thermodynamic model to chlorides after 91 days of hydration. The used data for Alite, Belite and Metakaolin after 91 days of hydration is not provided within the publication (Shi, Geiker, De Weerdt, *et al.*, 2017b). The reactivity for the remaining components (Fe_2O_3, SO_3, K_2O, Na_2O, MgO, $CaSO_4$, $NaCl$ and CO_2) has to be assumed giving a particular uncertainty. The initial assumptions, with inclusion of the data at 180 days, are scaled down until accordance to Shi et al.'s initial phase assemblage data is reached to a satisfying degree. Graphical data has been extracted by a digital tool for better comparison (Rohatgi, 2019). A list with the ions considered for the specific thermodynamic modelling done, can be found in the Appendix (list A).

Exposing the simulated materials to $NaCl$ and $CaCl_2$ solution of same concentrations used in the experiments considering the modified Langmuir isotherms for physical binding (based on experimental observations) allows to asses the impact of the implementation before and after the chemical solver is run.

Table 12: Combined DOH for different Materials after 180 days, initial model input

	wPc (P) DOH %	combination MK and wPc (ML) DOH %	combination MK and wPc (M) DOH %
CaO	89.9	89.9	89.9
SiO2	86.8	72.9	75.1
Al2O3	100	68.4	68.4

4. Results and Discussion

Calculating and fitting the data for physical bound chloride to the modified Langmuir expression leads to following physical chloride binding isotherms (Figure 8).
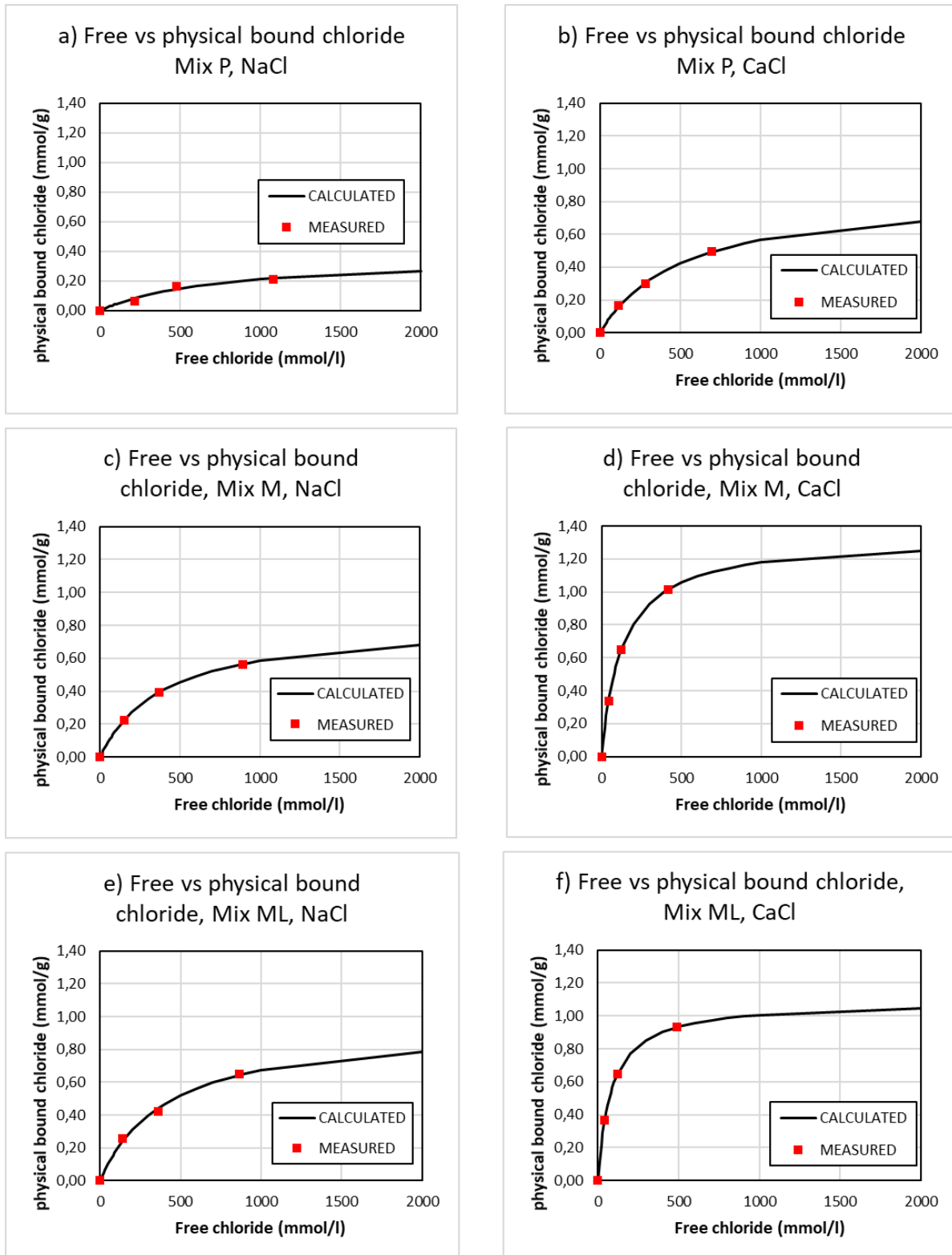
Figure 8: Free vs. physical bound chloride for P = pure Portland cement, M = partly substituted with Metakaolin, ML = partly substituted with Metakaolin and limestone

The resulting modified Langmuir binding parameter calculated for the different mixes are given in Table 13. In general, it can be observed that mixtures exposed to $CaCl_2$ show a higher physical binding capacity than mixtures of the same composition exposed to $NaCl$ solution of same chloride concentration (Figure 8). This is true for all three mixtures. It also appears that the physical binding capacity for $CaCl_2$ exposure increases faster in lower concentrations e.g. the curvature of the isotherm is steeper. The influence of the Cation, especially increased binding under the presence of calcium cations, is one of the major findings of Shi's investigation (Shi, Geiker, De Weerdt, *et al.*, 2017b). However, physical binding was not the focus of that investigation. The before mentioned observations become more clear in a direct comparison of the physical binding isotherms as shown in Figure 9.

Table 13 calculated Langmuir binding parameter

	α	β	x
P NaCl	0.005	0.014	0.1
P CaCl2	0.008	0.010	0.2
ML NaCl	0.023	0.024	0.1
ML CaCl2	0.131	0.121	0.1
M NaCl	0.021	0.025	0.1
M CaCl2	0.102	0.077	0.1
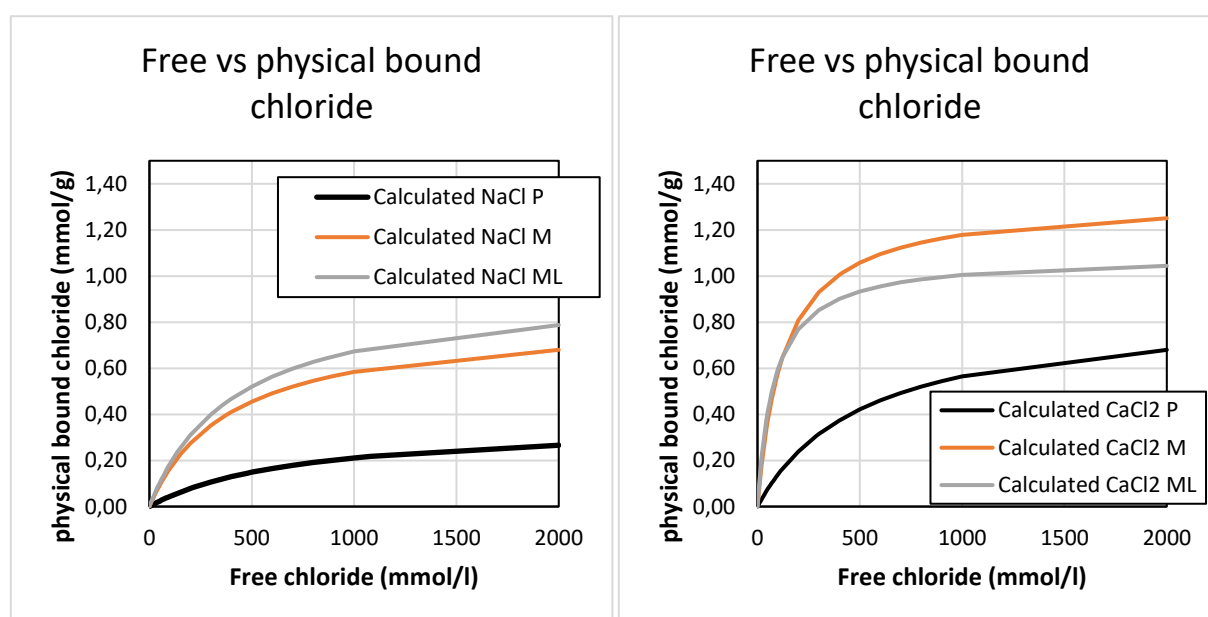
Figure 9: Modified Langmuir isotherms, comparison of the different materials

The difference between the physical binding capacity of the pure wPc binder and the binder with cement substitution is around a factor of three for $NaCl$ exposure and around two for $CaCl_2$ exposure. The physical binding capacity for the binder containing limestone and metakaolin appears to be slightly higher under $NaCl$ exposure, but slightly lower under $CaCl_2$ exposure compared to the binder containing only Metakaolin. Comparing the initial modelled phase assemblage to the phase assemblage of Shi et al. shows good agreement (Figure 10). There is a certain difference in the initial phase composition compared to the data retrieved from Shi's plots by a digitilizing tool. However, the results show a satisfying degree of comparability for the initial assemblage as shown in Table 14.
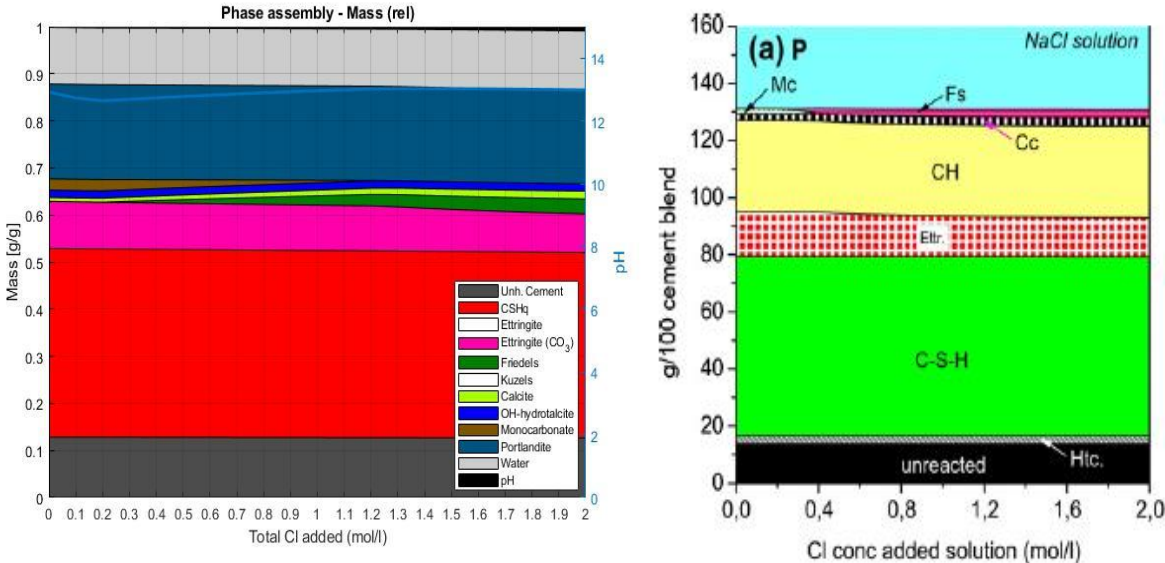
Figure 10 Modelled phase assemblage comparison to Shi et al. (Shi, Geiker, De Weerdt, et al., 2017a)

Table 14 comparison of initial phase composition (0 mol/l exposure)

	Mix P NaCl		Mix M NaCl		Mix ML NaCl	
Wt.%	Shi	model	Shi	model	Shi	model
CSH	39	40	37	40	37	42
Ettringite	10	10	4	3	7	7
Mono carbonate			11	11	16	16
CH	20	20				
Unreacted	9	12	19	20	16	16
Strängliitite			5	10		

Comparing the phase assemblage (Figure 11) it can be observed that for all mixes the chloride bearing phases e.g. Friedel's and Kunzel's salt are formed in a greater amount upon $CaCl_2$ exposure. Kunzel's salt is only predicte to form in mixture M at low chloride concentrations, which is in allingment with Shi's predicted phase assemblage upon exposure.
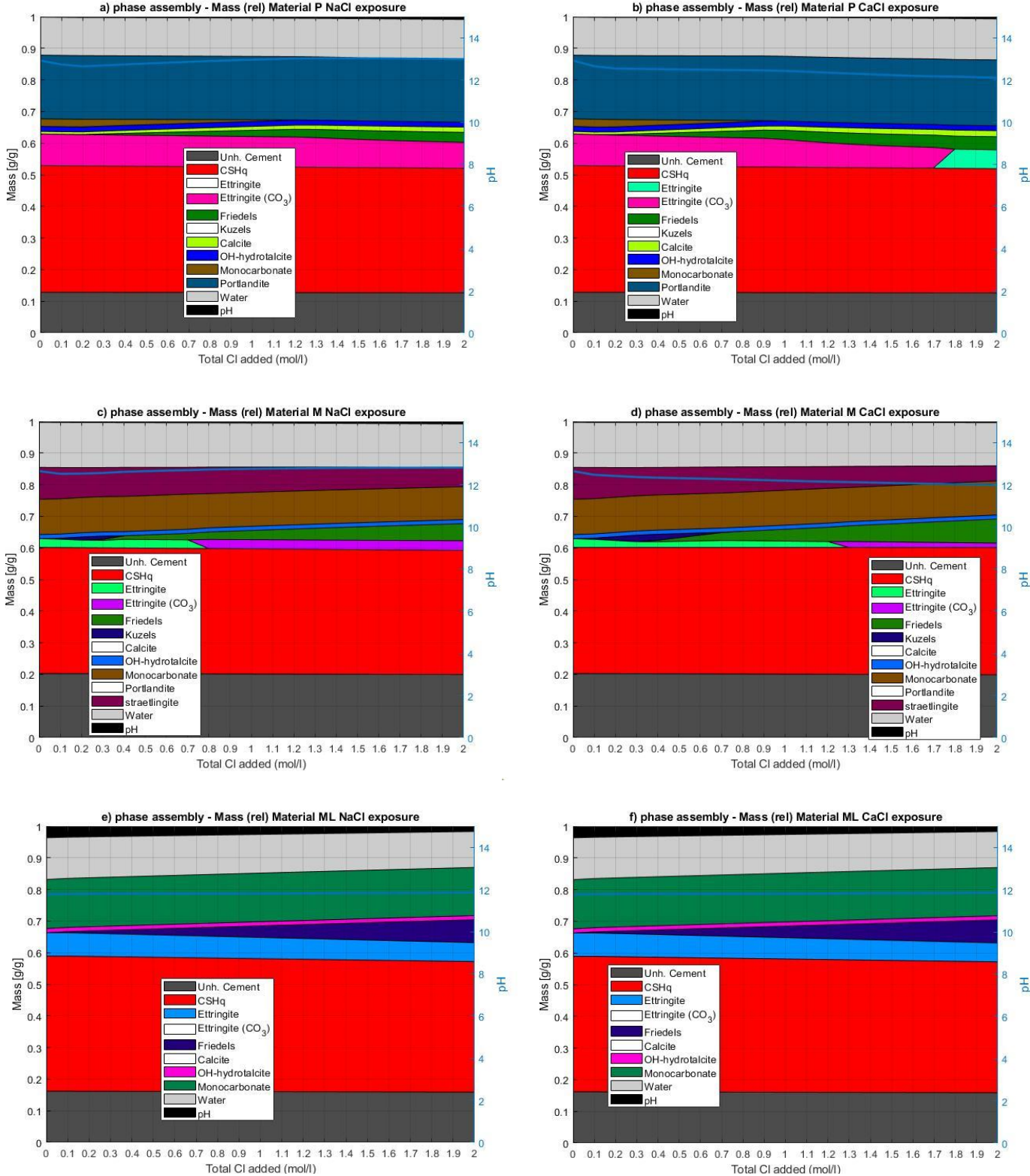
Figure 11 phase assemblage of the materials under different exposure conditions

Table 15 wt.% of predicted bound & free chlorides of the total chlorides at an exposure level of 2 mol/l; Mix P, M and ML

	Mix P no physical binding		Mix M no physical binding		Mix ML no physical binding	
	NaCl	CaCl2	NaCl	CaCl2	NaCl	CaCl2
chemical bound wt.%	48	63	69	97	96	100
physical bound wt.%	-	-	-	-	-	-
free chlorides wt.%	52	37	31	3	4	0

Table 15 exemplifies the observed amount of chlorides predicted by thermodynamic modelling to be bound chemical and available free in solution with the exposure solution at its peak of two mol/l of chloride exposure.

So far, the physical binding has not been considered. As explained in Section 3.2 the physical binding has been included before and after the chemical solver is run. Including the physical binding before the chemical solver is run leads to the distribution of predicted bound and free chlorides as shown in Figure 12. In the case of $NaCl$ exposure, the majority of the bound chloride is predicted to be bound physical (Figure 12 a, c and e) and only a minor part is predicted to be bound chemical. In case of $CaCl_2$ exposure of Mixture P, more chloride is predicted to be bound chemical (Figure 12 b). For Mixture M more chlorides are predicted to be free in solution for $NaCl$ exposure. For $CaCl_2$ exposure of Mixture M (Figure 12 d), the calculated amount of chemical bound chloride is less than for NaCl exposure but remains comparable. Almost no free chlorides are predicted to be in solution. The amount of physical bound chloride is predicted to be identical for both exposure conditions of mixture ML (Figure 12 e, f). No free chlorides are calculated to be in the solution. A summary in terms of wt.% of the bound chloride including physical binding before the chemical solver is given in following table:

Table 16 wt.% of predicted bound & free chlorides of the total chlorides at an exposure level of 2 mol/l including physical binding before chemical solver; Mix P, M and ML

	Mix P physical binding before		Mix M physical binding before		Mix ML physical binding before	
	NaCl	CaCl2	NaCl	CaCl2	NaCl	CaCl2
chemical bound wt.%	2	11	6	3	12	12
physical bound wt.%	62	84	85	97	88	88
free chlorides wt.%	36	5	9	0	0	0
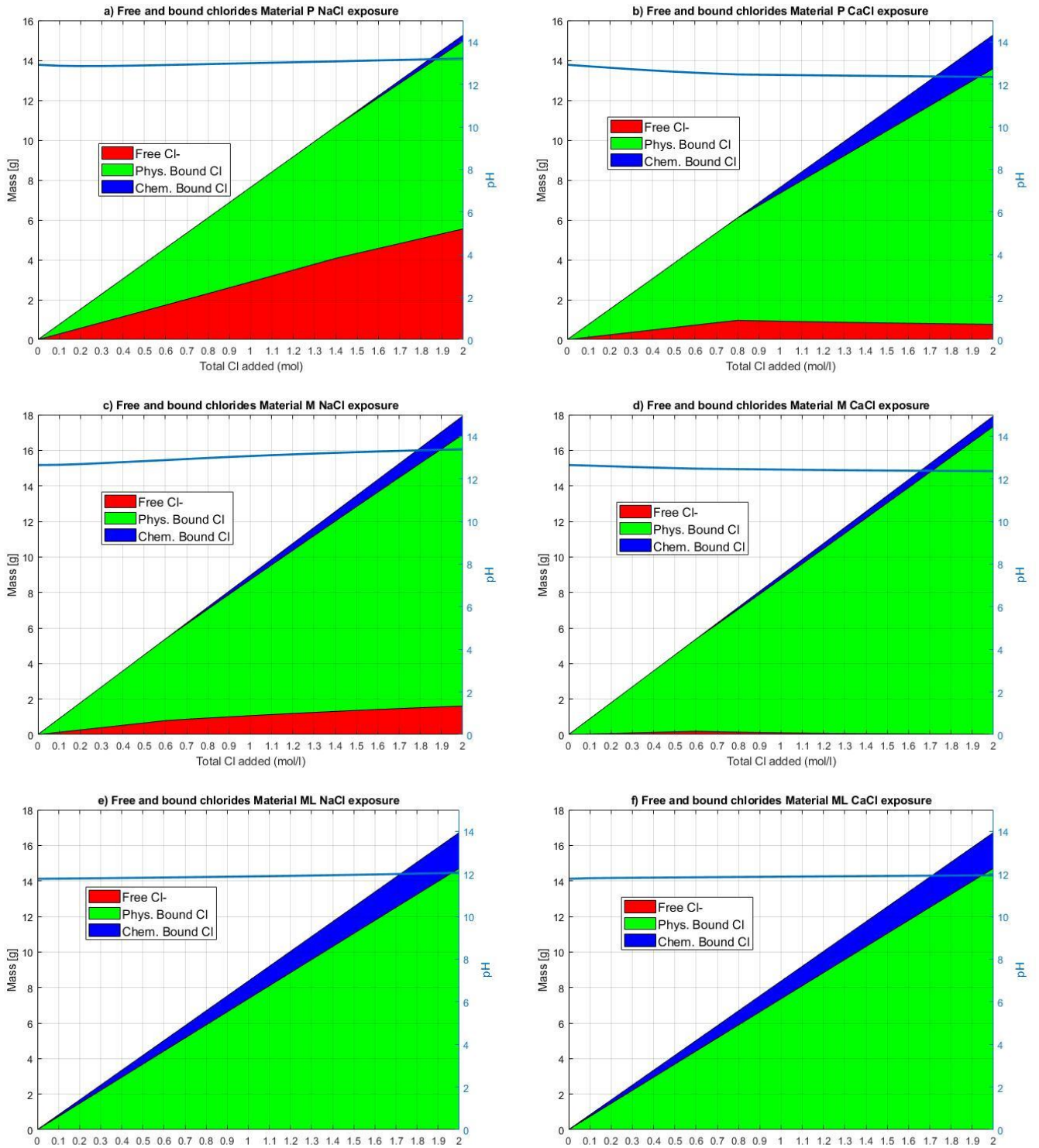
Figure 12 predicted bound & free chlorides including physical binding before chemical solver

If chemical binding is considered after the chemical solver is run the distribution is calculated as shown in Figure 13:
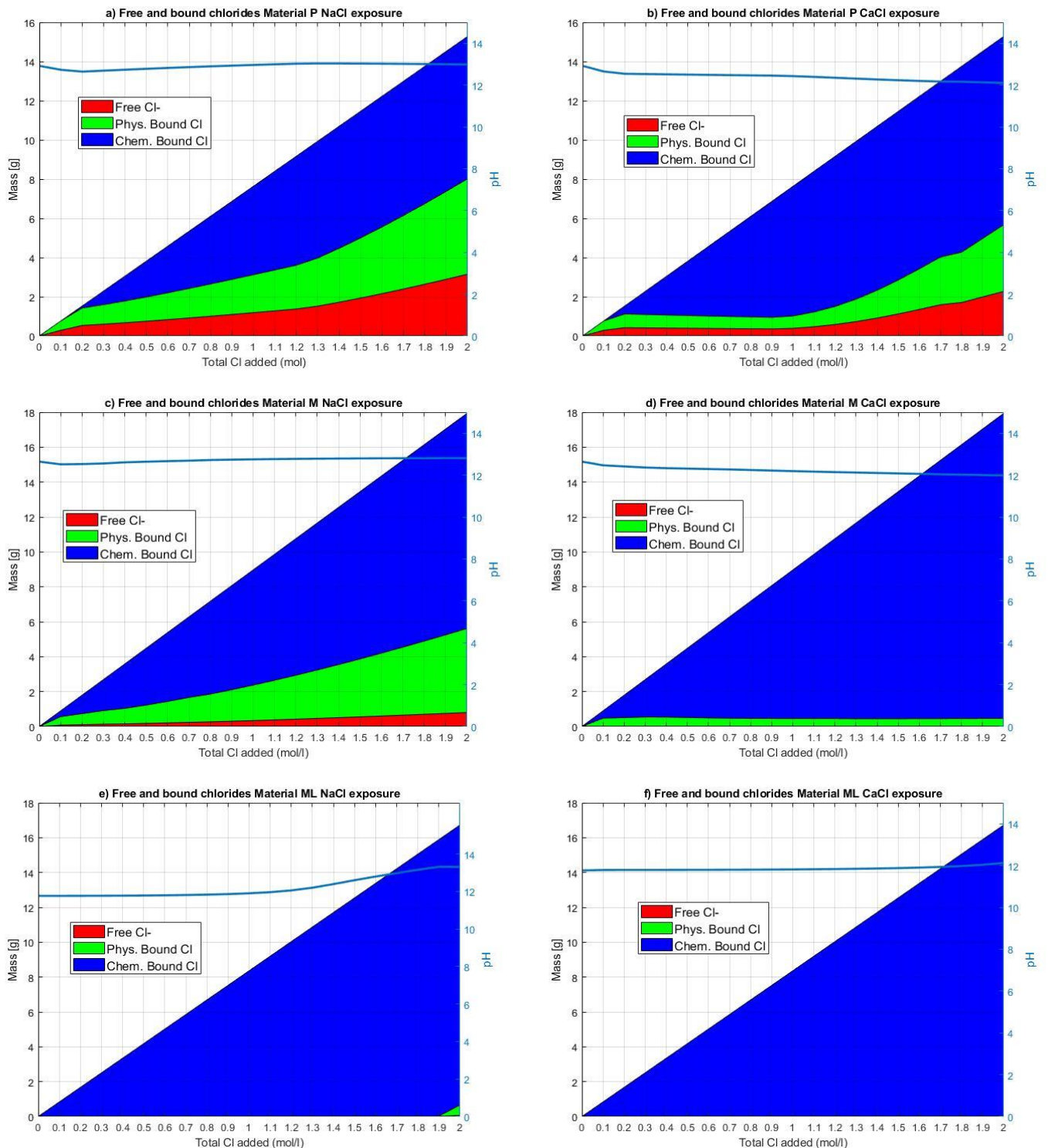
Figure 13 predicted bound & free chlorides including physical binding after chemical solver

In this case considering the $NaCl$ exposure a significant amount of chlorides is predicted to be bound physical for Mixture P and M (Figure 13 a,c), but the bigger share is predicted to be bound chemical (b,d). In case of the $CaCl_2$ exposure of the pure wPc mixture, physical bound chloride is predicted, but the amount is smaller than in the case of $NaCl$ exposure (Figure 13 e,f). For the mixtures containing metakaolin substitution, almost all chloride is predicted to be bound chemical and no free chloride is predicted in solution. For the Mixture ML there is only for $NaCl$ exposure a minor part of chlorides predicted to be free in solution (Figure 13 e). For $CaCl_2$ exposure all chlorides are bound (Figure 13 f). In both cases, no physical binding is predicted at all and all bound chloride is calculated to be bound chemical.

The inclusion of the physical binding also has implications on the phase assemblage as it changes the chlorides available for reaction. The biggest impact is found in mixture M exposed to $CaCl_2$ solution. In the phase assemblage, no more formation of Friedel's salt is predicted if the physical binding is included before the chemical solver. Kunzel's salt is predicted to form up to the maximum exposure concentration of two mol/l. Without physical binding Kunzel's salt was only predicted to be formed up to an exposure concentration of 0.7 mol/l (Figure 14). Comparisons of Mixture P with $NaCl$ and $CaCl_2$ exposure as well as Mixture M under $NaCl$ exposure are shown in in figure A1 (Appendices). A summary in terms of wt.% of the bound chloride including physical binding after the chemical solver is given in Table 17:

Table 17 wt.% of predicted bound & free chlorides of the total chlorides at an exposure level of 2 mol/l incl. physic. bin. after chemical solver; Mix P, M and ML

	Mix P physical binding after		Mix M physical binding after		Mix ML physical binding after	
	NaCl	CaCl2	NaCl	CaCl2	NaCl	CaCl2
chemical bound wt.%	48	63	69	97	96	100
physical bound wt.%	32	22	27	3	0	0
free chlorides wt.%	21	15	5	0	4	0
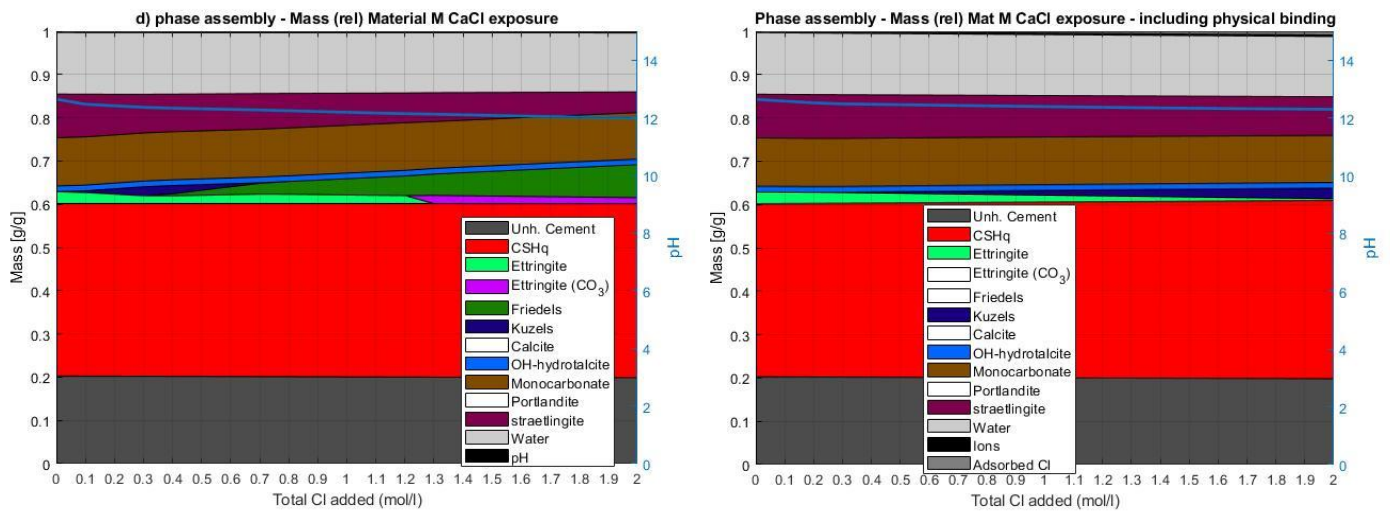
Figure 14 left: Mix M, CaCl2 exposure, no physical binding right: Mix M, CaCl2 exposure, physical binding before chemical solver

The big difference in physical binding capacity, has initially thought to be attributable to differences in C-S-H content. But as shown in Figure 11 there are no major differences between the C-S-H content predicted by thermodynamic modelling. Therefore, the physical binding is clearly not solely dependent on the C-S-H content of the material. In Section 2.1.1, it has been mentioned that the structure of C-S-H is dependent on the Ca/Si ratio. If cement is substituted with metakaolin there is clearly an increased amount of Si present in the initial mix composition. This will have an impact on the C-S-H itself. Also the pH-value, which is not identical for any of the mixtures (see Figure 11) will have an impact on the C-S-H if leaching occurs. Even though the C-S-H content might be comparable, the structure of it does not allow comparing it in terms of the physical binding capacity.

Including physical binding as a modified Langmuir isotherm based on experimental data, helps to get an idea about the impact on the phase assemblage and occurring binding. However, the results show that the physical binding included with this approach does not necessarily reflect the reality. This can simply be explained by the nature of the process and modelling sequence. If the physical binding is included before the chemical solver is run, a certain amount of chlorides is considered to be bound already and does not participate in formation of any phases. If on the other hand physical binding is included after the chemical solver is run, all chlorides are first considered to be available for phase formation and only the remaining chlorides (if there are any) will be considered according to the Langmuir expression. Thus, running the

43

physical binding after running the chemical solver leads to an underestimation of physical binding (as seen in e.g. Figure 13). If the physical binding is run before the chemical solver function, the chemical binding will be underestimated (see e.g. Figure 12). In reality, chemical and physical binding will occur at the same time. This cannot be represented by the used approach. The true resulting distribution between chemical and physical bound chloride might therefore lay somewhere in between the predictions done with a chemical solver run before and after considering the modified Langmuir isotherm. Results of this study indicate that there is no generic isotherm that can be used for every material. This can already be identified in Figure 9. Figure 11 shows that the assemblage of the materials is not identical and material parameters and assemblage as well as exposure conditions differ too much. This leads to very different predicted binding conditions as can be seen e.g. in Figure 12 and Figure 13.

Considering the modelling, inclusion of a surface complexation term as introduced in Section 2.3.1 might lead to less space for interpretation e.g. a result that lays between the values of the approach discussed above. The surface complexation approach also considers the Ca/Si ratio and the pH-value of the solution. Experimental data might therefore not be necessary.

Initial simulation of surface complexation in PHREEQC showed that uncertainty of the surface site density (which is not agreed upon by the scientific community) might not have a major impact on bound chlorides compared to other factors, when a cementitious system is simulated. With an exposure of 2.0 moles of NaCl and assumed surface site density of 4.787 sites/nm^2 as proposed by (Yogarajah, Nawa and Kurumisawa, 2018) 0.875 moles of Cl ions are calculated to be bound in the diffuse layer. Increasing the surface site density to 7 sites/nm^2 only increases the chloride in the diffuse layer to 0.878 moles. Simulating the same system for a 2 moles CaCl$_2$ exposure leads to a calculated amount of 1.434 moles chloride in the diffuse layer with assumed 4.787 sites/nm^2. Increasing that number to 7 sites/nm^2 leads to a calculated amount of 1.788 moles chloride in the diffuse layer. That difference is substantial but clearly the impact of the exposure condition and material properties has an impact that is several times higher. The present of calcium changed the surface charge by several magnitudes, but overcharging is not predicted for the simulated system. Exclusion of internal surface species e.g. surface sites that act bridging within the material matrix changes the amount of calculated chloride in the diffuse layer by 0.02 moles for NaCl and 0.01 moles for CaCl$_2$ exposure. This is a difference of two percent for NaCl and one percent for CaCl$_2$ exposure. With the given uncertainty in the input parameters in true surface area and exact composition this can be assumed to be neglectable. Leaving out the internal description can therefore save processing time without a major change

in the calculated results if the surface complexation approach is implemented. The PHREEQC input statements with the specified surface sites that were considered, and the structure of the cementitious system is included in the Appendix, calculations are based on the CEMDATA 18 database.

5. Conclusion

Based on literature research two different approaches have been identified to include physical chloride binding into an existing model. A methodology for modelling of each of these approaches has been presented. As the focus was on implementation of physical chloride binding by means of a modified Langmuir expression this implementation has been calibrated and tested against short-term data. The impact of the modelling sequence has been investigated. Upon the presented results and literature, several conclusions can be made.

1. Physical chloride binding is not solely dependent on the C-S-H content of the material, which will be exposed to chlorides. Dependency on C-S-H content has been assumed by several authors and might only be applicable for a range of very specific material compositions and exposure conditions. C-S-H composition is dependent on e.g. the Ca/Si ratio of the initial material and the pH-value due to leaching. Both therefore have an impact on the physical binding capacity. It has been explained that also the cation of the exposure solution has a huge impact at same chloride concentrations.

2. Review and calibration against experimental data showed that there is not a single Langmuir expression that can reflect the behaviour of a wide range of materials. This connects to Point 1. and the specific parameters of materials and exposure conditions. The Langmuir expression can only reflect specific conditions.

3. Inclusion of the modified Langmuir expression requires experimental data to calibrate. If the calibrated Langmuir isotherm is used in a sequenced model approach it will not necessarily reflect reality as it leads to an a) underestimation or b) overestimation of physical bound chloride depending on the modelling sequence (inclusion of the physical binding before or after the chemical solver is run in the single step sequenced model) and impacts thereby the predicted phase assemblage.

6. Recommendations for further work

This thesis showed that implementation of physical binding by means of the modified Langmuir expression requires experimental work for calibration and if it is applied in a single step modelled framework can only be used to reflect an overestimated or underestimated impact of physical binding. A methodology for surface complexation has been presented. This surface complexation might lead to more realistic values as it considers the impact of pH changes, associated cations and material structure by e.g. Ca/Si ratio. It is therefore suggested to compare results received and presented in this thesis with results obtained by an implementation of the surface complexation of the same material composition. For that matter all necessary material parameters should be included within this work. Initial PHREEQC based simulation showed that

- The impact of the material parameters and exposure conditions is several magnitudes higher than the impact of assumption on the surface site density which is also not agreed upon by the scientific community and certainly not the same for every material composition
- Exclusion of several equations describing internal site species does impact the result to degree that can be neglected, given the uncertainty of the input parameters and therefore save computational power and time

Literature

Addassi, M. *et al.* (2019) 'MODELLING AND TESTING OF CARBONATION EFFECTS ON HYDRATED OIL-WELL CEMENTS', in IFFSAR (ed.) *International Workshop. CO2 Storage in Concrete*. Marne La Vallée, FR.

Alkan, M. *et al.* (2005) 'Zeta potentials of perlite samples in various electrolyte and surfactant media', *Colloids and Surfaces A: Physicochemical and Engineering Aspects*, 259(1–3), pp. 155–166. doi: 10.1016/j.colsurfa.2005.02.024.

Balonis, M. *et al.* (2010) 'Impact of chloride on the mineralogy of hydrated Portland cement systems', *Cement and Concrete Research*. Elsevier Ltd, 40(7), pp. 1009–1022. doi: 10.1016/j.cemconres.2010.03.002.

Baroghel-bouny, V. *et al.* (2012) 'Prediction of chloride binding isotherms of cementitious materials by analytical model or numerical inverse analysis', *Cement and Concrete Research*. Elsevier Ltd, 42(9), pp. 1207–1224. doi: 10.1016/j.cemconres.2012.05.008.

Baroghel-Bouny, V. (2007) 'Water vapour sorption experiments on hardened cementitious materials. Part I: Essential tool for analysis of hygral behaviour and its relation to pore structure', *Cement and Concrete Research*, 37(3), pp. 414–437. doi: 10.1016/j.cemconres.2006.11.019.

Brunauer, S., Emmett, P. H. and Teller, E. (1938) 'Adsorption of Gases in Multimolecular Layers', *Journal of the American Chemical Society*, 60(2), pp. 309–319. doi: 10.1021/ja01269a023.

Chen, J. J. *et al.* (2004) 'Solubility and structure of calcium silicate hydrate', *Cement and Concrete Research*, 34(9), pp. 1499–1519. doi: 10.1016/j.cemconres.2004.04.034.

Cong, X. and Kirkpatrick, J. (1996) 'Si MAS NMR Study of the Structure of Calcium Silicate Hydrate', *Advn. Cem. Bas. Mat.*, 3, pp. 144–156.

Dilnesa, B. Z. *et al.* (2011) 'Iron in carbonate containing AFm phases', *Cement and Concrete Research*. Elsevier Ltd, 41(3), pp. 311–323. doi: 10.1016/j.cemconres.2010.11.017.

Dzombak, D. A. and Morel, F. M. M. (1990) *Surface Complexation Modeling: Hydrous Ferric Oxide*. A Wiley Interscience Publication.

Elakneswaran, Y., Nawa, T. and Kurumisawa, K. (2009) 'Electrokinetic potential of hydrated cement in relation to adsorption of chlorides', *Cement and Concrete Research*. Elsevier B.V., 39(4), pp. 340–344. doi: 10.1016/j.cemconres.2009.01.006.

Fidjestöl, P. and Tuutti, K. (1995) 'The importance of chloride diffusion', in *Proceedings of the RILEM Workshop on Chloride Penetration into Concrete*. Saint-Remy, France.

Glass, G. K. and Buenfeld, N. R. (2000) 'The influence of chloride binding on the chloride induced corrosion risk in reinforced concrete', *Corrosion Science*, 42(2), pp. 329–344. doi: 10.1016/S0010-938X(99)00083-9.

Glasser, F. P., Marchand, J. and Samson, E. (2008) 'Durability of concrete — Degradation phenomena involving detrimental chemical reactions', *Cement and Concrete Research*, 38(2), pp. 226–246. doi: 10.1016/j.cemconres.2007.09.015.

Grunewald, John; Häupl, Peter; Bomberg, M. (2003) 'Towards an engineering model of material characteristics for input to ham transport simulations - Part 1: An approach', *Journal of Thermal Envelope and Building Science*, 26(4).

Heath, T. G., D. J. Ilett, C. J. T. (1996) 'Thermodynamic Modelling of the sorption of

radioelements onto cementitious materials', *Mat. Res. Soc. Symp. Proc.*, 412, pp. 443–449.

Helene Viallis-Terrisse, Andre Nonat, and J.-C. P. (2001) 'Zeta-Potential Study of Calcium Silicate Hydrates Interacting with Alkaline Cations', *Journal of Colloid and Interface Science*, 244, pp. 58–65. doi: 10.1006/jcis.2001.7897.

Hemstad, P., Machner, A. and De Weerdt, K. (2020) 'The effect of artificial leaching with HCl on chloride binding in ordinary Portland cement paste', *Cement and Concrete Research*, 130(September 2019). doi: 10.1016/j.cemconres.2020.105976.

Hencoq, P. (2006) 'Modeling of ionic interactions at the C-S-H surface. Application to CsCl and LiCl solutions in comparison with NaCl solutions', in *Symposium on Advances in Concrete through Science and Enineering*. Quebec City.

Hiemstra, T. and Van Riemsdijk, W. H. (1996) 'A Surface Structural Approach to Ion Adsorption : The Charge Distribution (CD) Model', *Journal of Colloid and Interface Science*, 179, pp. 488–508.

Hirao, H. *et al.* (2005) 'Chloride Binding of Cement Estimated by Binding Isotherms of Hydrates', *Journal of Advanced Concrete Technology*, 3(1), pp. 77–84.

Hosokawa, Y. *et al.* (2006) 'MODELS FOR CHLORIDE ION BINDINGS IN HARDENED CEMENT', in *2nd International Symposium on Advances in Concrete through Science and Engineering*. Quebec City.

Janssen, H., Blocken, B. and Carmeliet, J. (2007) 'Conservative modelling of the moisture and heat transfer in building components under atmospheric excitation', *International Journal of Heat and Mass Transfer*, 50(5–6), pp. 1128–1140. doi: 10.1016/j.ijheatmasstransfer.2006.06.048.

Jensen, M. M. (2014) 'A Coupled Transport and Chemical Model for Durability Predictions of Cement Based Materials'. PhD thesis, Technical University of Denmark, 321(September), p. 208.

Jensen, M. M. *et al.* (2015) 'Use of a multi-species reactive transport model to simulate chloride ingress in mortar exposed to NaCl solution or sea-water', *Computational Materials Science*. Elsevier, 105, pp. 75–82. doi: 10.1016/J.COMMATSCI.2015.04.023.

Jensen, M. M., Johannesson, B. and Geiker, M. R. (2015) 'A Numerical Comparison of Ionic Multi-Species Diffusion with and without Sorption Hysteresis for Cement-Based Materials', *Transport in Porous Media*. Springer Netherlands, 107(1), pp. 27–47. doi: 10.1007/s11242-014-0423-3.

Jensen, M. M. M., Johannesson, B. and Geiker, M. R. R. (2014) 'Framework for reactive mass transport: Phase change modeling of concrete by a coupled mass transport and chemical equilibrium model', *Computational Materials Science*. Elsevier, 92, pp. 213–223. doi: 10.1016/j.commatsci.2014.05.021.

Johannesson, B. (2010) 'Development of a generalized version of the Poisson-Nernst-Planck equations using the hybrid mixture theory: Presentation of 2D numerical examples', *Transport in Porous Media*, 85(2), pp. 565–592. doi: 10.1007/s11242-010-9578-8.

Kulik, D. A. (2011) 'Improving the structural consistency of C-S-H solid solution thermodynamic models', *Cement and Concrete Research*. Elsevier Ltd, 41(5), pp. 477–495. doi: 10.1016/j.cemconres.2011.01.012.

Kulik, D. A. *et al.* (2015) 'GEMS: Gibbs Energy Minimization Software for geochemical modeling', p. 12. Available at: http://gems.web.psi.ch/contribs/GEMS-talk-Sep-2015.pdf.

Labbez, C. *et al.* (2007) 'Experimental and theoretical evidence of overcharging of calcium silicate hydrate', *Journal of Colloid and Interface Science*, 309(2), pp. 303–307. doi: 10.1016/j.jcis.2007.02.048.

Leidheiser, H. (1981) *Comprehensive treatise of electrochemistry. 1. The double layer*, *Journal of Colloid and Interface Science*. doi: 10.1016/0021-9797(81)90366-0.

Lippens, B. C., Linsen, B. G. and Boer, J. H. d. (1964) 'Studies on pore systems in catalysts I. The adsorption of nitrogen; apparatus and calculation', *Journal of Catalysis*, 3(1), pp. 32–37. doi: 10.1016/0021-9517(64)90089-2.

Lothenbach, B. *et al.* (2008) 'Thermodynamic modelling of the effect of temperature on the hydration and porosity of Portland cement', *Cement and Concrete Research*, 38(1), pp. 1–18. doi: 10.1016/j.cemconres.2007.08.017.

Lothenbach, B. *et al.* (2019) 'Cemdata18: A chemical thermodynamic database for hydrated Portland cements and alkali-activated materials', *Cement and Concrete Research*, 115, pp. 472–506. doi: 10.1016/j.cemconres.2018.04.018.

Lothenbach, B. and Winnefeld, F. (2006) 'Thermodynamic modelling of the hydration of Portland cement', *Cement and Concrete Research*, 36(2), pp. 209–226. doi: 10.1016/j.cemconres.2005.03.001.

Matschei, T., Lothenbach, B. and Glasser, F. P. (2007) 'Thermodynamic properties of Portland cement hydrates in the system CaO-Al2O3-SiO2-CaSO4-CaCO3-H2O', *Cement and Concrete Research*, 37(10), pp. 1379–1410. doi: 10.1016/j.cemconres.2007.06.002.

Mayant, C. *et al.* (2008) 'Surface site density, silicic acid retention and transport properties of compacted magnetite powder', *Physics and Chemistry of the Earth*, 33(14–16), pp. 991–999. doi: 10.1016/j.pce.2008.05.011.

Meson, V. M. (2019) *Reactive mass transport model for cement-based materials - parametric study*. Lyngby.

Michel, A. (2012) *Reinforcement Corrosion : Numerical Simulation and Service Life Prediction*.

Michel, A. *et al.* (2019) 'Coupled mass transport, chemical, and mechanical modelling in cementitious materials: A dual-lattice approach', in Caspeele, R., Taerwe, L., and Frangopol, D. M. (eds) *Life Cycle Analysis and Assessment in Civil Engineering: Towards an Integrated Vision: Proceedings of the Sixth International Symposium on Life-Cycle Civil Engineering (IALCCE 2018)*. Ghent, Belgium: CRC Press, pp. 965–972.

Mounanga, P. *et al.* (2004) 'Predicting Ca(OH)2 content and chemical shrinkage of hydrating cement pastes using analytical approach', *Cement and Concrete Research*, 34(2), pp. 255–265. doi: 10.1016/j.cemconres.2003.07.006.

Müller, R. H. (1996) *Zetapotential und Partikelladung in der Laborpraxis: Einführung in die Theorie, Praktische Meßdurchführung, Dateninterpretation*. Wissenschaftliche Verlagsgesellschaft.

Nguyen, T. Q., Baroghel-Bouny, V. and Dangla, P. (2006) 'Prediction of chloride ingress into saturated concrete on the basis of a multi-species model by numerical calculations', *Computers and Concrete*, 3(6), pp. 401–422. doi: 10.12989/cac.2006.3.6.401.

Nilsson, L. *et al.* (1996) 'Chloride Penetration Into Concrete State-of-the-art: Transport Processes, Corrosion Initiation, Test Methods and Prediction Models', (December 2015), p. 151. doi: 10.13140/RG.2.1.2771.7526.

Nonat, A. (2004) 'The structure and stoichiometry of C-S-H', *Cement and Concrete Research*, 34(9), pp. 1521–1528. doi: 10.1016/j.cemconres.2004.04.035.

Parkhurst, D. L. and Appelo, C. a. J. (2013) 'Description of Input and Examples for PHREEQC Version 3 — A Computer Program for Speciation , Batch-Reaction , One-Dimensional Transport , and Inverse Geochemical Calculations. U.S. Geological Survey Techniques and Methods, book 6, chapter A43, 497 p.', *U.S. Geological Survey Techniques and Methods, book 6, chapter A43*, pp. 6-43A.

Ping Yu, R. James Kirkpatrick, Brent Poe, P. F. M. and X. C. (1999) 'Structure of Calcium Silicate Hydrate (C-S-H): Near-, Mid-, and Far-Infrared Spectroscopy', *Journal of the American Ceramic Society*, 82, pp. 742–748.

Plassard, C. *et al.* (2005) 'Nanoscale Experimental Investigation of Particle', *Langmuir*, 21(16), pp. 7263–7270. doi: 10.1021/LA050440+.

Plusquellec, G. and Nonat, A. (2016) 'Interactions between calcium silicate hydrate (C-S-H) and calcium chloride, bromide and nitrate', *Cement and Concrete Research*. Elsevier Ltd, 90, pp. 89–96. doi: 10.1016/j.cemconres.2016.08.002.

Pointeau, I. *et al.* (2006) 'Measurement and modeling of the surface potential evolution of hydrated cement pastes as a function of degradation', *Journal of Colloid and Interface Science*, 300(1), pp. 33–44. doi: 10.1016/j.jcis.2006.03.018.

Poulsen, S. L. *et al.* (2009) 'Improved quantification of alite and belite in anhydrous Portland cements by 29Si MAS NMR: Effects of paramagnetic ions', *Solid State Nuclear Magnetic Resonance*, 36(1), pp. 32–44. doi: 10.1016/j.ssnmr.2009.05.001.

Richardson, I. G. (2004) 'Tobermorite / jennite- and tobermorite / calcium hydroxide-based models for the structure of C-S-H : applicability to hardened pastes of tricalcium silicate , h - dicalcium silicate , Portland cement , and blends of Portland cement with blast-furnace slag ', *Cement and Concrete Research*, 34, pp. 1733–1777. doi: 10.1016/j.cemconres.2004.05.034.

Rohatgi, A. (2019) *WebPlotDigitizer 4.2*, *WebPlotDigitizer*. Available at: https://automeris.io/WebPlotDigitizer.

Scheffler, G. A. and Plagge, R. (2010) 'A whole range hygric material model: Modelling liquid and vapour transport properties in porous media', *International Journal of Heat and Mass Transfer*. Elsevier Ltd, 53(1–3), pp. 286–296. doi: 10.1016/j.ijheatmasstransfer.2009.09.030.

Schirmer, R. (1938) 'Die Diffusionszahl von Wasserdampf-Luft-Gemischen und die Verdampfungsgeschwindigkeit (german)'. Berlin: VDI-Verlag.

Shi, Z., Geiker, M. R., Lothenbach, B., *et al.* (2017a) 'Friedel's salt profiles from thermogravimetric analysis and thermodynamic modelling of Portland cement-based mortars exposed to sodium chloride solution', *Cement and Concrete Composites*. Elsevier, 78, pp. 73–83. doi: 10.1016/j.cemconcomp.2017.01.002.

Shi, Z., Geiker, M. R., Lothenbach, B., *et al.* (2017b) 'Friedel's salt profiles from thermogravimetric analysis and thermodynamic modelling of Portland cement-based mortars exposed to sodium chloride solution', *Cement and Concrete Composites*. Elsevier Ltd, 78, pp. 73–83. doi: 10.1016/j.cemconcomp.2017.01.002.

Shi, Z., Geiker, M. R., De Weerdt, K., *et al.* (2017a) 'Role of calcium on chloride binding in hydrated Portland cement–metakaolin–limestone blends', *Cement and Concrete Research*. Elsevier Ltd, 95, pp. 205–216. doi: 10.1016/j.cemconres.2017.02.003.

Shi, Z., Geiker, M. R., De Weerdt, K., *et al.* (2017b) 'Role of calcium on chloride binding in

hydrated Portland cement–metakaolin–limestone blends', *Cement and Concrete Research*. Pergamon, 95, pp. 205–216. doi: 10.1016/j.cemconres.2017.02.003.

Stern, O. (1924) 'Zur Theorie der Elektrolytischen Doppelschicht', *Zeitschrift fur Elektrochemie*, 30, pp. 508–516. doi: 10.1002/bbpc.192400182.

Tang, L. and Nilsson, L.-O. (1993) 'Chloride Binding Capacity and Binding Isotherms of OPC Pastes and Mortars', *Cement and Concrete Research*, 23, pp. 247–253.

Taylor, H. F. W. (1993) 'Nanostructure of CSH: Current status', *Advanced Cement Based Materials*, 1(1), pp. 38–46. doi: 10.1016/1065-7355(93)90006-A.

Thiéry, M. and Wang, X. (2011) 'Modelling of isothermal coupled moisture – ion transport in cementitious materials', *Cement and Concrete Research*. Elsevier Ltd, 41(8), pp. 828–841. doi: 10.1016/j.cemconres.2011.04.001.

Tritthart, J. (1989) 'Chloride binding in cement II. The influence of the hydroxide concentration in the pore solution of hardened cement paste on chloride binding', *Cement and Concrete Research*, 19, pp. 683–691.

Vignisdottir, H. R. *et al.* (2016) 'Life Cycle assessment of Anti-and De-icing Operations in Norway', *CIB World Building Congress*, (June), pp. 441–454.

Weerdt, K. De *et al.* (2015) 'Impact of the associated cation on chloride binding of Portland cement paste', *Cement and Concrete Research*. Elsevier Ltd, 68, pp. 196–202. doi: 10.1016/j.cemconres.2014.01.027.

Ye, H. *et al.* (2016) 'Prediction of chloride binding isotherms for blended cements', *Computers and Concrete*, 17(5), pp. 655–672. doi: 10.12989/cac.2016.17.5.655.

yoga, E. *et al.* (2010) 'Ion-cement hydrate interactions govern multi-ionic transport model for cementitious materials', *Cement and Concrete Research*, 40(12), pp. 1756–1765. doi: 10.1016/j.cemconres.2010.08.019.

Yogarajah, E., Nawa, T. and Kurumisawa, K. (2018) 'Influence of surface electrical properties of C-S-H on chloride binding in slag-blended cementitious materials', *Journal of Materials in Civil Engineering*. American Society of Civil Engineers (ASCE), 30(5). doi: 10.1061/(ASCE)MT.1943-5533.0002263.

Appendix

OH-, H+, AlO2-, AlO2H, AlSiO5-3, AlO+, Al(OH)+2, Al+3, Al(SO4)+, Al(SO4)2-, AlHSiO3+2, Ca(OH)+,Ca+2, CaSO4, CaCO3, CaSiO3, Ca(HCO3)+, Ca(HSiO3)+, FeO2-, FeO2H, FeO+, Fe(OH)+2, FeOH+, Fe+2, FeCO3, Fe(SO4), Fe+3, FeCl+, FeCl+2, FeCl2+, FeCl3, K+, KOH, KSO4-, Mg(OH)+, Mg+2, Mg(SO4), Mg(CO3), MgSiO3, Mg(HCO3)+, Mg(HSiO3)+, NaOH, Na+, Na(SO4)-, NaCO3-, NaHCO3, SiO3-2, SiO2, SO4-2, HSO4-, CO2, CO3-2, HCO3-, Cl-

list A1 considered ions in thermodynamic modelling

Table A1 constants for chloride calculations

Constants			
w/b		0,95	-
Molar mass of Cl		35,45	g/mol
Free water wt% of wet paste	P	30,4	%
	ML	29,5	%
	M	31,4	%
Volume exposure solution		15,00	mL
Mass wet paste per sample		30,00	g
Mass paste per sample	P	20,88	g
	ML	21,15	g
	M	20,58	g
WPC per cement paste	P	100,00	wt%
	ML	68,10	wt%
	M	68,10	wt%
WPC in each sample	P	20,88	g
	ML	14,22	g
	M	14,22	g
Free water from paste in each sample	P	9,12	ml
	ML	8,85	ml
	M	9,42	ml

Table A2 added, free and equilibrium chloride concentrations

NaCl	P		ML		M	
$C_{Cl,added}$	$C_{Cl,free}$	$C_{Cl,eq}$	$C_{Cl,free}$	$C_{Cl,eq}$	$C_{Cl,free}$	$C_{Cl,eq}$
mol/l	mol/l	mol/l	mol/l	mol/l	mol/l	mol/l
2,000	1,244	1,078	1,258	0,862	1,229	0,892
1,000	0,622	0,476	0,629	0,359	0,614	0,369
0,500	0,311	0,213	0,314	0,137	0,307	0,152
0,250	0,155	0,081	0,157	0,036	0,154	0,047
0,125	0,078	0,031	0,079	0,012	0,077	0,012
0,000	0,000	0,001	0,000	0	0,000	0,001

CaCl2	P		ML		M	
$C_{Cl,added}$	$C_{Cl,free}$	$C_{Cl,eq}$	$C_{Cl,free}$	$C_{Cl,eq}$	$C_{Cl,free}$	$C_{Cl,eq}$
Conc.	mol/l	mol/l	mol/l	mol/l	mol/l	mol/l
2,000	1,244	0,695	1,258	0,491	1,229	0,419
1,000	0,622	0,285	0,629	0,123	0,614	0,122
0,500	0,311	0,114	0,314	0,042	0,307	0,045
0,250	0,155	0,047	0,157	0,012	0,154	0,017
0,125	0,078	0,019	0,079	0,005	0,077	0,005
0,000	0,000	0	0,000	0	0,000	0,000

Table A3 amount of Friedel's salt (g/g cement) for the different mixes and exposure conditions (Shi, Geiker, De Weerdt, *et al.*, 2017b)

	P-CaCl2	P-NaCl	ML-CaCl2	ML-NaCl	M-CaCl2	M-NaCl
0,00	0	0	0	0	0	0
0,10	0	0	0	0	0	0
0,20	0,001476	0	0,001138	0	0	0
0,30	0,002747	0,000839	0,004635	0	0,001137	0
0,40	0,003045	0,002436	0,00813	0,001192	0,010667	0
0,50	0,003216	0,002673	0,011626	0,002493	0,014597	0
0,80	0,003429	0,003073	0,022113	0,006148	0,021967	0,012072

1,00	0,003477	0,003221	0,029104	0,00852	0,028933	0,013782
1,50	0,003514	0,003417	0,032988	0,014539	0,037278	0,016956
2,00	0,003522	0,003498	0,033098	0,020874	0,037465	0,019324

Table A4 amount of total bound chloride (g/g paste) for the different mixes and exposure conditions (Shi, Geiker, De Weerdt, *et al.*, 2017b)

NaCl		P	CaCl2		P
$C_{Cl,added}$	$C_{Cl,bound}$		$C_{Cl,added}$	$C_{Cl,bound}$	
Conc,	average	SD	Conc,	average	SD
2	0,011	0,001	2	0,021	0
1	0,009	0,001	1	0,014	0
0,5	0,005	0	0,5	0,009	0
0,25	0,004	0	0,25	0,005	0
0,125	0,003	0	0,125	0,003	0
0	0	0	0	0	0
NaCl		ML	CaCl2		ML
$C_{Cl,added}$	$C_{Cl,bound}$		$C_{Cl,added}$	$C_{Cl,bound}$	
Conc,	average	SD	Conc,	average	SD
2	0,023	0,001	2	0,033	0,001
1	0,015	0	1	0,023	0
0,5	0,009	0	0,5	0,013	0
0,25	0,007	0	0,25	0,007	0
0,125	0,004	0	0,125	0,004	0
0	0	0	0	0	0
NaCl		M	CaCl2		M
$C_{Cl,added}$	$C_{Cl,bound}$		$C_{Cl,added}$	$C_{Cl,bound}$	
Conc,	average	SD	Conc,	average	SD
2	0,02	0	2	0,036	0
1	0,014	0,001	1	0,023	0
0,5	0,008	0	0,5	0,012	0
0,25	0,006	0	0,25	0,007	0

0,125	0,004	0	0,125	0,003	0
0	0	0	0	0	0

Table A5 calculated amount of physical bound chloride

Mix P	NaCl					Mix P	CaCl2			
$C_{Cl,added}$	$C_{Cl,final}$	$C_{Cl,physical}$				$C_{Cl,added}$	$C_{Cl,final}$	$C_{Cl,physical}$		
Conc,	mol/L	mmol/L	g/g	mmol/g		Conc,	mol/L	mmol/L	g/g	mmol/g
2	1,078	1078	0,01	0,21		2	0,695	695	0,02	0,49
1	0,476	476	0,01	0,16		1	0,285	285	0,01	0,30
0,5	0,213	213	0,00	0,07		0,5	0,114	114	0,01	0,16
0,25	0,081	81				0,25	0,047	47		
0,125	0,031	31				0,125	0,019	19		
0	0,001	1	0,00	0,00		0	0	0	0,00	0,00

Mix ML	NaCl					Mix ML	CaCl2			
$C_{Cl,added}$	$C_{Cl,final}$	$C_{Cl,physical}$				$C_{Cl,added}$	$C_{Cl,final}$	$C_{Cl,physical}$		
Conc,	mol/L	mmol/L	g/g	mmol/g		Conc,	mol/L	mmol/L	g/g	mmol/g
2	0,862	862	0,02	0,65		2	0,491	491	0,03	0,93
1	0,359	359	0,02	0,42		1	0,123	123	0,02	0,65
0,5	0,137	137	0,01	0,25		0,5	0,042	42	0,01	0,37
0,25	0,036	36				0,25	0,012	12		
0,125	0,012	12				0,125	0,005	5		
0	0	0	0,00	0,00		0	0	0	0,00	0,00

Mix M	NaCl					Mix M	CaCl2			
$C_{Cl,added}$	$C_{Cl,final}$	$C_{Cl,physical}$				$C_{Cl,added}$	$C_{Cl,final}$	$C_{Cl,physical}$		
Conc,	mol/L	mmol/L	g/g	mmol/g		Conc,	mol/L	mmol/L	g/g	mmol/g
2	0,892	892	0,02	0,56		2	0,419	419	0,04	1,02
1	0,369	369	0,01	0,39		1	0,122	122	0,02	0,65
0,5	0,152	152	0,01	0,23		0,5	0,045	45	0,01	0,34
0,25	0,047	47				0,25	0,017	17		

0,125	0,012	12			0,125	0,005	5		
0	0,001	1	0,00	0,00	0	0	0	0,00	0,00

Table A6 reactivity (ALPHA) used for thermodynamic modelling of different species

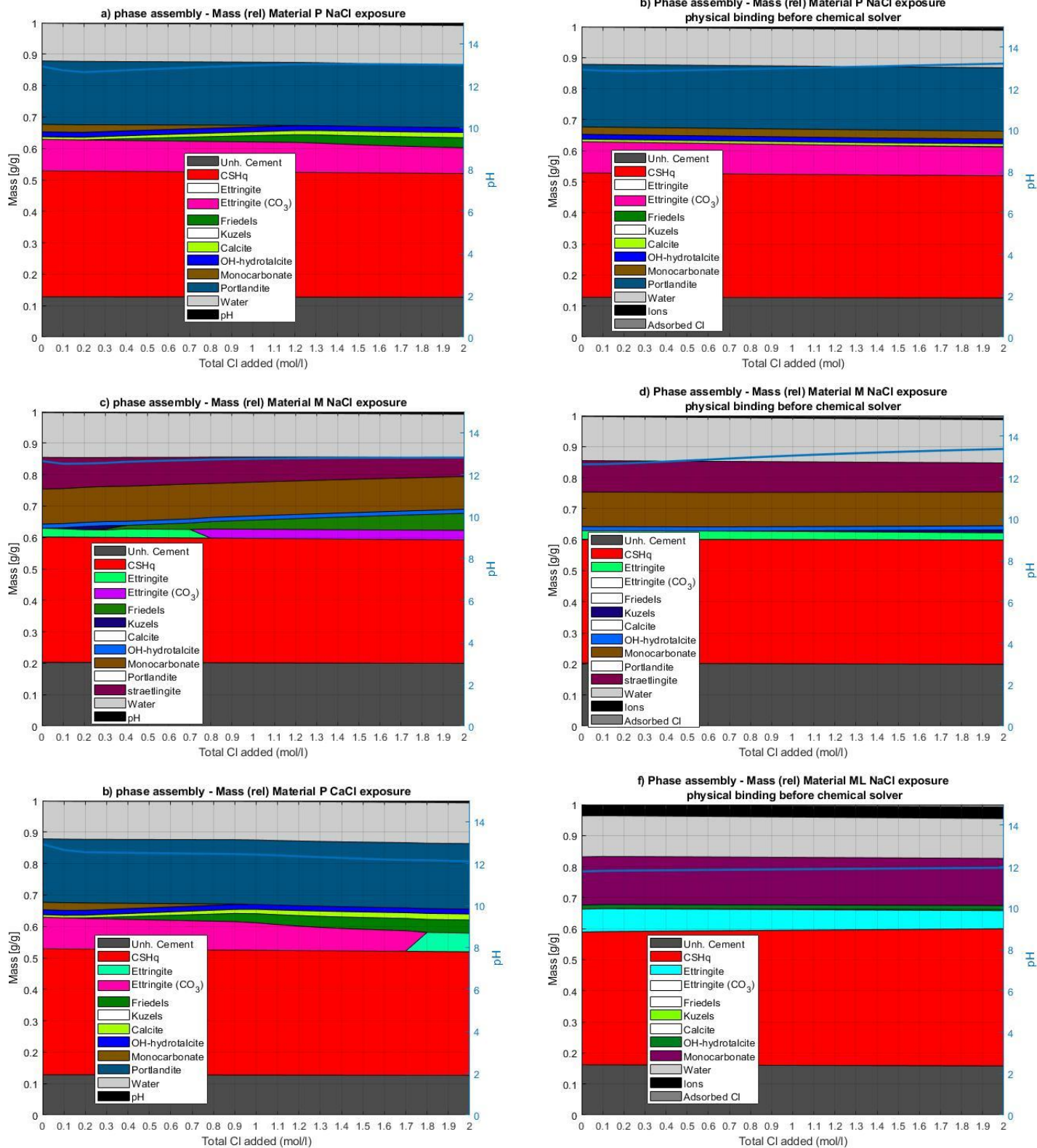| ALPHA		Material P	Material ML	Material M
CaO	-	0,85	0,85	0,82
SiO2	-	0,83	0,68	0,68
Al2O3	-	0,7	0,7	0,5
Fe2O3	-	0,4	0,4	0,4
SO3	-	0,28	0,4	0,2
K2O	-	0,8	0,8	0,8
Na2O	-	0,8	0,8	0,8
MgO	-	0,8	0,8	0,8
CaSO4	-	0,5	0,5	0,2
Cl	-	0	0	0
CO2	-	1	1	1

Figure A1 Phase assemlby comparison with and without inclusion of physical binding before the chemical solver

Table A7 possible ions, oxides and equilibrium phases to consider in the solving process

ID	OXIDE	ION	EQ	ID	ION	EQ
1	CaO	OH-	'CH4(g)'	70	CH4	'Fe-hemicarbonate'
2	SiO2	H+	'CO2(g)'	71	CO3-2	'Fe-monosulph05'
3	Al2O3	O2	'H2(g)'	72	HCO3-	'Fe-monosulphate'
4	Fe2O3	H2	'H2O(g)'	73	Cl-	'Fe'
5	SO3	AlO2-	'H2S(g)'	74	ClO4-	'Femonocarbonate'
6	K2O	AlO2H	'N2(g)'	75	NH4+	'FeOOHmic'
7	Na2O	AlSiO5-3	'O2(g)'	76	N2	'Gbs'
8	MgO	AlO+	'5CA'	77	NO3-	'Gp'
9	CaSO4	Al(OH)+2	'5CNA'	78	NH3	'Gr'
10	Cl	Al+3	'AlOHam'	79	HCN	'Gt'
11	CO2	Al(SO4)+	'AlOHmic'	80	SCN-	'Hem'
12		Al(SO4)2-	'Amor-Sl'	81		'hemicarbonat10.5'
13		AlHSiO3+2	'Anh'	82		'hemicarbonate'
14		Ca(OH)+	'Arg'	83		'hemicarbonate9'
15		Ca+2	'Brc'	84		'hemihydrate'
16		CaSO4	'C2AClH5'	85		'hydrotalcite'
17		CaCO3	'C2AH7.5'	86		'INFCA'
18		CaSiO3	'C2AH65'	87		'INFCN'
19		Ca(HCO3)+	'C2S'	88		'INFCNA'
20		Ca(HSiO3)+	'C3A'	89		'Jennite'
21		FeO2-	'C3AFS0.84H4.32'	90		'K2O'
22		FeO2H	'C3AH6'	91		'K2SO4'
23		FeO+	'C3AS0.41H5.18'	92		'Kln'
24		Fe(OH)+2	'C3AS0.84H4.32'	93		'KSiOH'
25		FeOH+	'C3FH6'	94		'Lim'
26		Fe+2	'C3FS0.84H4.32'	95		'M4A-OH-LDH'
27		FeCO3	'C3FS1.34H3.32'	96		'M6A-OH-LDH'
28		Fe(SO4)	'C3S'	97		'M8A-OH-LDH'
29		Fe+3	'C4AClH10'	98		'Mag'
30		Fe(SO4)+	'C4AF'	99		'Melanterite'

31	FeHCO3+	'C4AH11'	100	'Mg2AlC0.5OH'
32	FeHSiO3+2	'C4AH13'	101	'Mg2FeC0.5OH'
33	Fe(SO4)2-	'C4AH19'	102	'Mg3AlC0.5OH'
34	FeHSO4+	'C4AsClH12'	103	'Mg3FeC0.5OH'
35	FeHSO4+2	'C4FH13'	104	'Mgs'
36	Fe2(OH)2+4	'C12A7'	105	'monocarbonate05'
37	Fe3(OH)4+5	'CA2'	106	'monocarbonate9'
38	FeCl+	'CA'	107	'monocarbonate'
39	FeCl+2	'CAH10'	108	'mononitrate'
40	FeCl2+	Cal'	109	'mononitrite'
41	FeCl3	'Cls'	110	'monosulphate9'
42	K+	'CSH3T-T2C'	111	'monosulphate10_5'
43	KOH	'CSH3T-T5C'	112	'monosulphate12'
44	KSO4-	'CSH3T-TobH'	113	'monosulphate14'
45	Mg(OH)+	'CSHQ-JenD'	114	'monosulphate16'
46	Mg+2	'CSHQ-JenH'	115	'monosulphate1205'
47	Mg(SO4)	'CSHQ-TobD'	116	'Na2O'
48	Mg(CO3)	'CSHQ-TobH'	117	'Na2SO4'
49	MgSiO3	'Dis-Dol'	118	'NaSiOH'
50	Mg(HCO3)+	'ECSH1-KSH'	119	'Ord-Dol'
51	Mg(HSiO3)+	'ECSH1-NaSH'	120	'Portlandite'
52	NaOH	'ECSH1-SH'	121	'Py'
53	Na+	'ECSH1-SrSH'	122	'Qtz'
54	Na(SO4)-	'ECSH1-TobCa'	123	'Sd'
55	NaCO3-	'ECSH2-JenCa'	124	'straetlingite5_5'
56	NaHCO3	'ECSH2-KSH'	125	'straetlingite7'
57	SiO3-2	'ECSH2-NaSH'	126	'straetlingite'
58	HSiO3-	'ECSH2-SrSH'	127	'Str'
59	SiO2	'ECSH2-TobCa'	128	'Sulfur'
60	Si4O10-4	'ettringite'	129	'syngenite'
61	HS-	'ettringite03_ss'	130	'T2C-CNASHss'
62	S2O3-2	'ettringite05'	131	'T5C-CNASHss'

63	SO3-2	'ettringite9'	132	'thaumasite'
64	SO4-2	'Ettringite9_des'	133	'Tob-I'
65	HSO4-	'ettringite13'	134	'Tob-II'
66	H2S	'Ettringite13_des'	135	'TobH-CNASHss'
67	HSO3-	'ettringite30'	136	'tricarboalu03'
68	S-2	'Fe-ettringite05'	137	'Tro'
69	CO2	'Fe-ettringite'	138	Fe(OH)3am'

PHREEQC composition and surface site description example:

```
SOLID_SOLUTIONS 1
    CSHQ
    component CSHQ-JenD 1.554953E+00
    component CSHQ-JenH 8.543291E-01
    component CSHQ-TobD 1.154623E+00
    component CSHQ-TobH 3.992287E-02
    component KSiOH 3.710691E-01
    component NaSiOH 3.127481E+00
    C3(AF)S0.84H
    component C3AFS0.84H4.32 3.365754E-01
    component C3FS0.84H4.32 6.838743E-02
    ettringite
    component ettringite 1.123740E-01
    component ettringite30 3.839081E-02
    SO4_CO3_AFt
    component tricarboalu03 0.000000E+00
    component ettringite03_ss 0.000000E+00
SURFACE 1
    equilibrate with solution 1
    sites_units density
    Sio_e       4.787        600        25           Dw 0
    Sio_i       4.787
    diffuse_layer 1e-08
    only_counter_ions
SURFACE_MASTER_SPECIES
    Sio_i         Sio_iOH#internal check for effect if not considered
    Sio_e         Sio_eOH
SURFACE_SPECIES
Sio_eOH = Sio_eOH
    log_k      0
Sio_iOH = Sio_iOH
    log_k      0
Sio_eOH = Sio_eO- + H+
    log_k      -11.8
Ca+2 + Sio_eOH = Sio_eOCa+ + H+
    log_k      -9
Ca(OH)+ + Sio_eOH = Sio_eOCaOH + H+
    log_k      -12
0.5SiO2 + H2O + Sio_eOH = Sio_eOSi0.5OH + H2O
    log_k      3.5
0.5Ca+2 + Sio_eOSi0.5OH = Sio_eOSi0.5OCa0.5 + H+
```

```
     log_k     -10.2
Sio_eOSi0.5OH = Sio_eOSi0.5O- + H+
     log_k     -11.8
Ca+2 + Sio_eOSi0.5OH = Sio_eOSi0.5OCa+ + H+
     log_k     -9
0.5Ca+2 + Sio_iOH = (Sio_iO)Ca0.5 + H+
     log_k     -10.2
Ca(OH)+ + Sio_iOH = Sio_iOCaOH + H+
     log_k     -12
0.5SiO2 + H2O + Sio_iOH = Sio_iOSi0.5OH + H2O
     log_k     3.5
0.5Ca+2 + Sio_iOSi0.5OH = Sio_iOSi0.5OCa0.5 + H+
     log_k     -10.2
Ca+2 + Cl- + Sio_eOH = Sio_eOCaCl + H+
     log_k     -8.9
Ca+2 + SO4-2 + Sio_eOH = Sio_eOCaSO4- + H+
     log_k     -6
0.5Ca+2 + Sio_iOH = (Sio_iO)Ca0.5 + H+
     log_k     -10.2
Ca(OH)+ + Sio_iOH = Sio_iOCaOH + H+
     log_k     -12
0.5SiO2 + H2O + Sio_iOH = Sio_iOSi0.5OH + H2O
     log_k     3.5
0.5Ca+2 + Sio_iOSi0.5OH = Sio_iOSi0.5OCa0.5 + H+
     log_k     -10.2
```